Differential geometry
Surfaces are studied in a branch of mathematics called *differential geometry*. The mathematicians study perfectly rigid surfaces and surfaces with no stiffness at all (topology) which is rather restrictive from our point of view. Nonetheless, many formulas in these notes are copied from books on differential geometry. Here are three useful formulas [8].

If an orthogonal parameterisation (p. 25) is available then the shell curvatures can be calculated with

$$k_{xx} = \left(\left(\frac{\partial \bar{y}}{\partial u}\frac{\partial \bar{z}}{\partial v} - \frac{\partial \bar{z}}{\partial u}\frac{\partial \bar{y}}{\partial v}\right)\frac{\partial^2 \bar{x}}{\partial u^2} + \left(\frac{\partial \bar{z}}{\partial u}\frac{\partial \bar{x}}{\partial v} - \frac{\partial \bar{x}}{\partial u}\frac{\partial \bar{z}}{\partial v}\right)\frac{\partial^2 \bar{y}}{\partial u^2} + \left(\frac{\partial \bar{x}}{\partial u}\frac{\partial \bar{y}}{\partial v} - \frac{\partial \bar{y}}{\partial u}\frac{\partial \bar{x}}{\partial v}\right)\frac{\partial^2 \bar{z}}{\partial u^2} \right)\frac{1}{\alpha_x^3 \alpha_y}$$

$$k_{yy} = \left(\left(\frac{\partial \bar{y}}{\partial u}\frac{\partial \bar{z}}{\partial v} - \frac{\partial \bar{z}}{\partial u}\frac{\partial \bar{y}}{\partial v}\right)\frac{\partial^2 \bar{x}}{\partial v^2} + \left(\frac{\partial \bar{z}}{\partial u}\frac{\partial \bar{x}}{\partial v} - \frac{\partial \bar{x}}{\partial u}\frac{\partial \bar{z}}{\partial v}\right)\frac{\partial^2 \bar{y}}{\partial v^2} + \left(\frac{\partial \bar{x}}{\partial u}\frac{\partial \bar{y}}{\partial v} - \frac{\partial \bar{y}}{\partial u}\frac{\partial \bar{x}}{\partial v}\right)\frac{\partial^2 \bar{z}}{\partial v^2} \right)\frac{1}{\alpha_x \alpha_y^3}$$

$$k_{xy} = \left(\left(\frac{\partial \bar{y}}{\partial u}\frac{\partial \bar{z}}{\partial v} - \frac{\partial \bar{z}}{\partial u}\frac{\partial \bar{y}}{\partial v}\right)\frac{\partial^2 \bar{x}}{\partial u \partial v} + \left(\frac{\partial \bar{z}}{\partial u}\frac{\partial \bar{x}}{\partial v} - \frac{\partial \bar{x}}{\partial u}\frac{\partial \bar{z}}{\partial v}\right)\frac{\partial^2 \bar{y}}{\partial u \partial v} + \left(\frac{\partial \bar{x}}{\partial u}\frac{\partial \bar{y}}{\partial v} - \frac{\partial \bar{y}}{\partial u}\frac{\partial \bar{x}}{\partial v}\right)\frac{\partial^2 \bar{z}}{\partial u \partial v} \right)\frac{1}{\alpha_x^2 \alpha_y^2}$$

where α_x and α_y are the Lamé parameters (p. 32).

Curvilinear coordinate system
In shell analysis three coordinate systems are used (fig. 43); 1) a global coordinate system (p. 19) to describe the shape of the shell, 2) a local coordinate system (p. 19) to define curvature, displacements, membrane forces, moments and loading, 3) a *curvilinear coordinate system* to derive and solve the shell equations.
The axis of the curvilinear coordinate system are *u* and *v*. They are plotted onto the shell middle surface. All lines of this coordinate system cross perpendicularly. It looks like a timber grid shell (see Savill building p. 22). The *x* direction in a point is tangent to the local *u* direction and the *y* direction in a point is tangent to the local *v* direction.

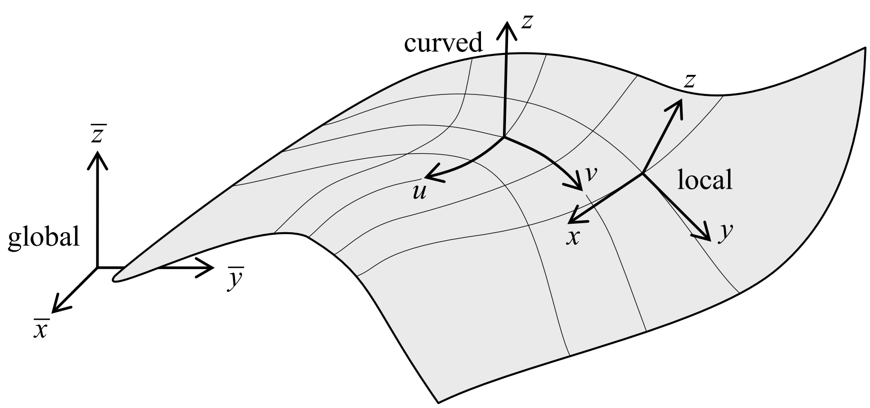

Figure 43. Coordinate systems

In the curvilinear coordinate system it is simple to locate any point (*u*, *v*) on the shell surface. Also, the positive directions of the membrane forces and moments are clear in any point. For example, consider the torus in figure 44. There is nothing unclear about the statement:

"At the location $(u,v)=(\frac{3}{2}\pi b,\frac{1}{2}\pi a)$ the membrane shear force is $n_{xy}=10$ kN/m ".

$$\bar{x}=(b+a\sin\frac{v}{a})\sin\frac{u}{b}$$

$$\bar{y}=(b+a\sin\frac{v}{a})\cos\frac{u}{b}$$

$$\bar{z}=a\cos\frac{v}{a}$$

$$0<v<2\pi a$$

$$0<u<2\pi b$$

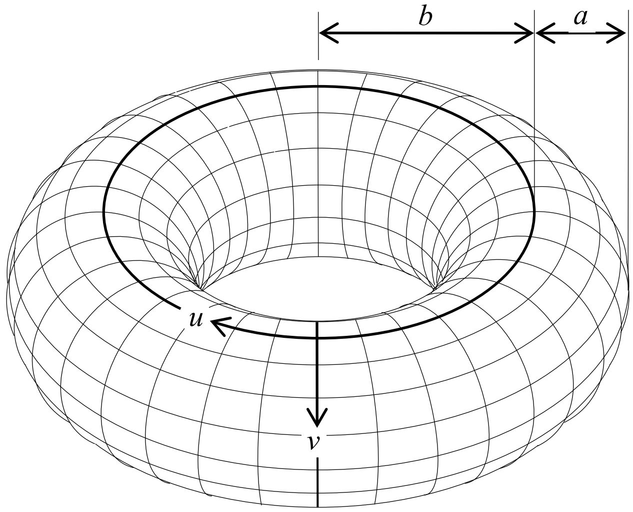

$$k_{xx}=\frac{-1}{a+\dfrac{b}{\sin\frac{v}{a}}}$$

$$k_{yy}=-\frac{1}{a}$$

$$k_{xy}=0$$

$$\alpha_x=1+\frac{a}{b}\sin\frac{v}{a}$$

$$\alpha_y=1$$

Figure 44. Curved coordinate system on a torus

Shell displacement and load
Every point of the shell middle surface has a local Cartesian coordinate system *x*, *y*, *z* (fig. 45). Every point has displacements u_x, u_y, u_z. Every point is loaded by distributed forces p_x, p_y, p_z [kN/m²].

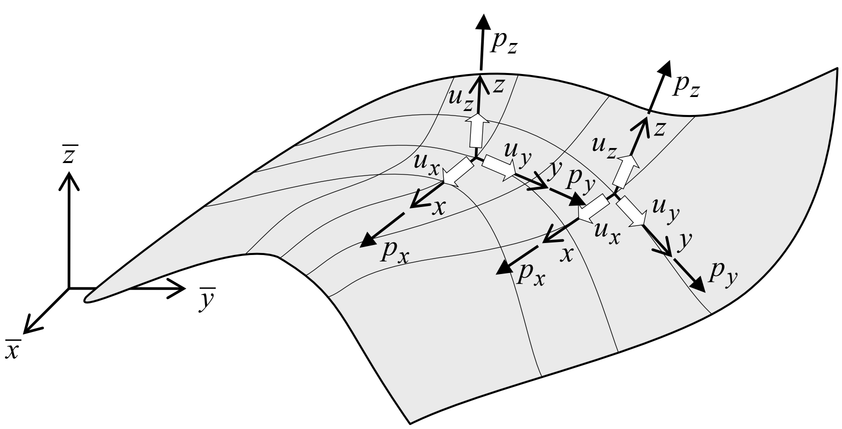

Figure 45. Displacements and loads

Lamé parameters
A complication of the curved coordinate system is that the distance between two grid lines varies from point to point. Therefore, a small length *dx* is often not the same as a small length *du*. For the torus in figure 44 we can derive

$$\begin{bmatrix} dx \\ dy \end{bmatrix}=\begin{bmatrix} 1+\frac{a}{b}\sin\frac{v}{a} & 0 \\ 0 & 1 \end{bmatrix}\begin{bmatrix} du \\ dv \end{bmatrix}.$$

Exercise: Derive these equations by inspection of the torus curved coordinate system.

In general we write

$$\begin{bmatrix} dx \\ dy \end{bmatrix} = \begin{bmatrix} \alpha_x & 0 \\ 0 & \alpha_y \end{bmatrix} \begin{bmatrix} du \\ dv \end{bmatrix},$$

where α_x and α_y are called *Lamé parameters*.[1] The inverse of the later equations is simply

$$\begin{bmatrix} du \\ dv \end{bmatrix} = \begin{bmatrix} \frac{1}{\alpha_x} & 0 \\ 0 & \frac{1}{\alpha_y} \end{bmatrix} \begin{bmatrix} dx \\ dy \end{bmatrix}.$$

Therefore, $\frac{\partial u}{\partial x} = \frac{1}{\alpha_x}$, $\frac{\partial v}{\partial y} = \frac{1}{\alpha_y}$, $\frac{\partial u}{\partial y} = 0$, $\frac{\partial v}{\partial x} = 0$. The Lamé parameters are important when differentiating. For example, if we differentiate the membrane shear force $n_{xy}(u,v)$ to x we need to use the chain rule

$$\frac{\partial n_{xy}}{\partial x} = \frac{\partial n_{xy}}{\partial u}\frac{\partial u}{\partial x} + \frac{\partial n_{xy}}{\partial v}\frac{\partial v}{\partial x} = \frac{\partial n_{xy}}{\partial u}\frac{1}{\alpha_x}.$$

If an orthogonal parameterisation (p. 25) is available then the Lamé parameters can be calculated with.

$$\alpha_x = \sqrt{\frac{\partial \bar{x}}{\partial u}^2 + \frac{\partial \bar{y}}{\partial u}^2 + \frac{\partial \bar{z}}{\partial u}^2},$$
$$\alpha_y = \sqrt{\frac{\partial \bar{x}}{\partial v}^2 + \frac{\partial \bar{y}}{\partial v}^2 + \frac{\partial \bar{z}}{\partial v}^2}.$$

The proof is simple. If we change u a bit then $\bar{x}$, $\bar{y}$ and $\bar{z}$ change a bit and the length of the latter bit follows from Pythagoras' theorem. Q.E.D.

Equation of Gauß

The Lamé parameters (p. 32) can be used to calculate Gaussian curvature (p. 23).

$$k_G = -\frac{1}{\alpha_y}\frac{\partial^2 \alpha_y}{\partial x^2} - \frac{1}{\alpha_x}\frac{\partial^2 \alpha_x}{\partial y^2}$$

[1] Gabriel Lamé (1795–1870) was a French mathematician who taught at universities in Saint Petersburg and in Paris [Wikipedia]

This is called the *equation of Gauß* [for a derivation see 9 p. 175]. Applying the chain rule this can be written as

$$k_G = -\frac{1}{\alpha_x \alpha_y}\left[\frac{\partial}{\partial u}\left(\frac{1}{\alpha_x}\frac{\partial \alpha_y}{\partial u}\right)+\frac{\partial}{\partial v}\left(\frac{1}{\alpha_y}\frac{\partial \alpha_x}{\partial v}\right)\right].$$

For example, the torus of figure 44 has a Gaussian curvature of

$$k_G = -\frac{1}{1+\frac{a}{b}\sin\frac{v}{a}}\left[0+\frac{\partial}{\partial v}\left(1\frac{\partial}{\partial v}(1+\frac{a}{b}\sin\frac{v}{a})\right)\right]=\frac{1}{a^2+\frac{ab}{\sin\frac{v}{a}}}.$$

Exercise: Are the shapes in table 2 completely determined?

Table 2. Examples of Lamé parameters (p. 32) that produce uniform Gaussian curvatures (p. 23) (Uniform means not a function of u and not a function of v.)

$\alpha_x = 1$	$\alpha_y = \sin\frac{u}{a}$	$k_G = \frac{1}{a^2}$	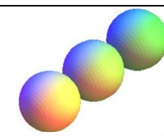 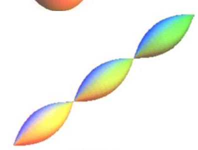
$\alpha_x = 1$	$\alpha_y = \cos\frac{u}{a}$	$k_G = \frac{1}{a^2}$	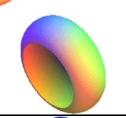
$\alpha_x = 1$	$\alpha_y = \cosh\frac{u}{a}$	$k_G = -\frac{1}{a^2}$	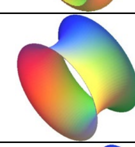
$\alpha_x = 1$	$\alpha_y = \sinh\frac{u}{a}$	$k_G = -\frac{1}{a^2}$	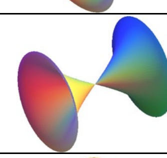
$\alpha_x = 1$	$\alpha_y = \exp\frac{u}{a}$	$k_G = -\frac{1}{a^2}$	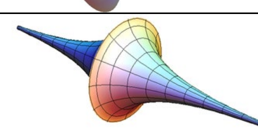
$\alpha_x = 1$	$\alpha_y = 1-\frac{Cu^2}{2}+\frac{C^2u^4}{4!}-\frac{C^3u^6}{6!}+\frac{C^4u^8}{8!}-\ldots$	$k_G = C$	
$\alpha_x = 1-\frac{Cv^2}{4}$	$\alpha_y = 1-\frac{Cu^2}{4}$	$k_G \approx C$	

Intrinsic property
Consider the sticker shown in figure 46. It has a length and width of 20 cm. The sticker material is very flexible. Subsequently, it is carefully glued onto a curved surface without wrinkles and cracks. The angles between the lines remain 90°. Figure 47 shows the stretched lengths of the sticker lines.

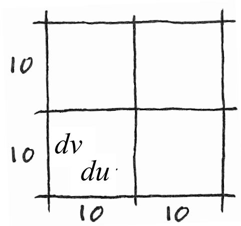

Figure 46. Sticker printed on a flexible material

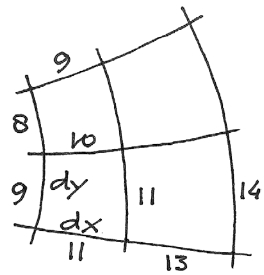

Figure 47. Sticker stretched onto a surface

The Lamé parameters (p. 32) are

$$\alpha_x = \frac{11\,\text{cm}}{10\,\text{cm}} = 1.1 \qquad \alpha_y = \frac{9\,\text{cm}}{10\,\text{cm}} = 0.9$$

$$\frac{\partial \alpha_x}{\partial v} = \frac{1.0 - 1.1}{10\,\text{cm}} = \frac{-0.01}{\text{cm}} \qquad \frac{\partial \alpha_y}{\partial u} = \frac{1.1 - 0.9}{10\,\text{cm}} = \frac{0.02}{\text{cm}}$$

Substitution in the equation of Gauß (p. 33) gives

$$k_G = -\frac{1}{1.1 \times 0.9}\left[\frac{\partial}{\partial u}\left(\frac{1}{1.1}\frac{0.02}{\text{cm}}\right) + \frac{\partial}{\partial v}\left(\frac{1}{0.9}\frac{-0.01}{\text{cm}}\right)\right]$$

$$= -\frac{1}{1.1 \times 0.9}\left[\frac{\frac{1}{1.3}\frac{0.03}{\text{cm}} - \frac{1}{1.1}\frac{0.02}{\text{cm}}}{10\,\text{cm}} + \frac{\frac{1}{0.8}\frac{-0.01}{\text{cm}} - \frac{1}{0.9}\frac{-0.01}{\text{cm}}}{10\,\text{cm}}\right] = -0.00035\,\frac{1}{\text{cm}^2}$$

Only surface measurements were used. Apparently, for calculating Gaussian curvature we need not measure the shell shape in three-dimensional space. For this reason, Gaussian curvature (p. 23) is called an *intrinsic* property. Mean curvature (p. 24) is not intrinsic.

Exercise: Do the sticker calculation with $k_G = -\frac{1}{\alpha_y}\frac{\partial^2 \alpha_y}{\partial x^2} - \frac{1}{\alpha_x}\frac{\partial^2 \alpha_x}{\partial y^2}$. It should produce the same result.

Curved roofs with tiles
Modern tile roofs are always flat. However, the length that tiles overlap can vary, which can be used to build curved roofs (fig. 48). Clearly, tiles should divert rain and stay on the roof in a storm. This imposes constraints to the slope of tiles. The particle-spring method (p. 105) can be used to determine a suitable grid.

Figure 48. Queens palace in Silinduang Bulan, Indonesia [10]
The curved roofs are made of flat tiles.

Equations of Codazzi
The equations of Codazzi are [9] [2]

$$\frac{\partial \alpha_x k_{xx}}{\partial y} = k_{yy} \frac{\partial \alpha_x}{\partial y}, \qquad \frac{\partial \alpha_y k_{yy}}{\partial x} = k_{xx} \frac{\partial \alpha_y}{\partial x}.$$

They are valid if x and y are the principal curvature directions, so $k_{xy} = 0$.

Apparently, we cannot create a shell by just choosing functions $k_{xx} = \ldots$, $k_{yy} = \ldots$, $k_{xy} = \ldots$, $\alpha_x = \ldots$ and $\alpha_y = \ldots$. Our choice must fulfil the equation of Gauß and the equations of Codazzi.

Helicoid
A helicoid (fig. 49) can be described by

$$\bar{x} = a\,v\cos u \qquad\qquad \bar{x} = a\sinh(u-v)\cos(u+v)$$
$$\bar{y} = a\,v\sin u \qquad \text{and by} \qquad \bar{y} = a\sinh(u-v)\sin(u+v)$$
$$\bar{z} = a\,u \qquad\qquad \bar{z} = a(u+v)$$

Its mean curvature (p. 24) is zero everywhere, therefore it is a minimal surface.

[2] Delfino Codazzi (1868–1869) was a mathematics professor at the University of Pavia, Italy. The Codazzi equations were also discovered by Gaspare Mainardi (1800–1879) and by Karl Mikhailovich Peterson (1828–1881). The latter seems to have been the first [Wikipedia].

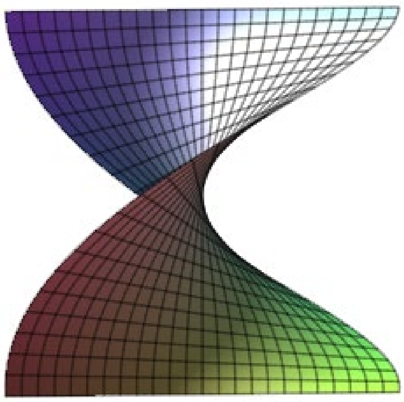

$$k_{xx} = 0$$
$$k_{yy} = 0$$
$$k_{xy} = \frac{1}{a(1+v^2)}$$
$$\alpha_x = a\sqrt{1+v^2}$$
$$\alpha_y = a$$

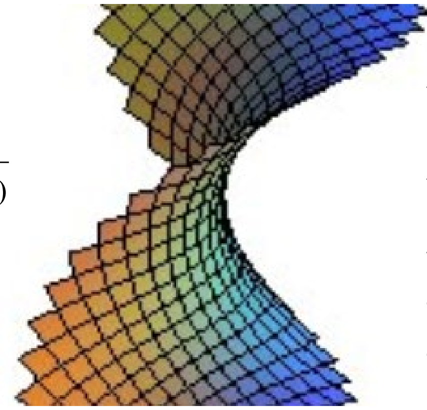

$$k_{xx} = \frac{-1}{a\cosh^2(u-v)}$$
$$k_{yy} = \frac{1}{a\cosh^2(u-v)}$$
$$k_{xy} = 0$$
$$\alpha_x = a\sqrt{2}\cosh(u-v)$$
$$\alpha_y = a\sqrt{2}\cosh(u-v)$$

$-\pi/2 < u < \pi/2 \qquad -\pi/2 < v < \pi/2 \qquad\qquad -\pi/2 < u + v < \pi/2 \qquad -\pi/2 < u - v < \pi/2$

Figure 49. Helicoid

Exercise: Check the equation of Gauß (p. 33) and the equations of Codazzi (p. 36) for a helicoid.

Challenge: It should be possible to generalise the equations of Codazzi to one equation that is valid for $k_{xy} \neq 0$ too.

In plane curvature

Figure 50 shows curved parameter lines on a curved surface. The lines have a radius of curvature r_y in the plane that is tangent to the shell middle surface. This radius can be expressed in the Lamé parameter α_x (p. 32). The proportions in the figure show that

$$\frac{\alpha_x\, du}{r_y} = \frac{\frac{\partial \alpha_x}{\partial y} du\, dy}{dy}. \qquad \Rightarrow \qquad \frac{1}{r_y} = \frac{1}{\alpha_x}\frac{\partial \alpha_x}{\partial y}$$

We define $k_x = \frac{1}{r_y}$, therefore, $k_x = \frac{1}{\alpha_x}\frac{\partial \alpha_x}{\partial y}$

In the same way can be defined $k_y = \frac{1}{\alpha_y}\frac{\partial \alpha_y}{\partial x}$.

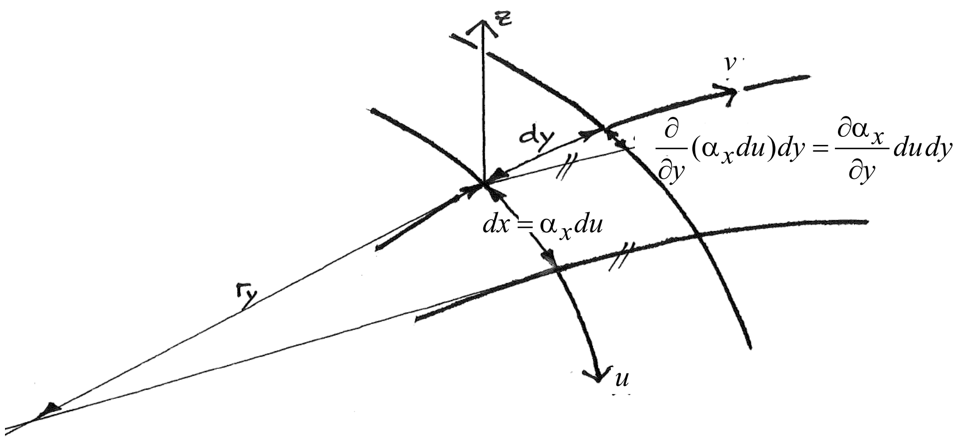

Figure 50. Radius r_y of the parameter line v = constant

Exercise: Derive that $k_G = -\frac{\partial k_x}{\partial y} - \frac{\partial k_y}{\partial x} - k_x^2 - k_y^2$

Challenge: Suppose we have two orthogonal parameterisations of a shell.
The local coordinate systems in a shell point are *x–y–z* and *r–s–z*. Proof or disproof that

$k_r = k_x \cos\varphi - k_y \sin\varphi$

$k_s = k_x \sin\varphi + k_y \cos\varphi$

where φ is the angle between the *r* axis and the *x* axis (see appendix 3).

Shell membrane equations

The shell membrane equations are shown in table 3. These equations describe the behaviour of thin shell structures, however, all moments have been neglected. Nonetheless, they are useful because for many shells the moments have little influence on their global behaviour. The shell equations that do include moments are called Sanders-Koiter equations (p. 54).

In these notes only the equilibrium equations and the kinematic equations are derived. The constitutive equations are the same as for flat plates loaded in plane. For their derivations see a course on plates.

Table 3. Shell membrane equations

kinematic equations	$\varepsilon_{xx} = \frac{\partial u_x}{\partial x} - k_{xx} u_z + k_x u_y$	1
	$\varepsilon_{yy} = \frac{\partial u_y}{\partial y} - k_{yy} u_z + k_y u_x$	2
	$\gamma_{xy} = \frac{\partial u_x}{\partial y} + \frac{\partial u_y}{\partial x} - 2k_{xy} u_z - k_x u_x - k_y u_y$	3
constitutive equations	$\varepsilon_{xx} = \frac{1}{E\,t}(n_{xx} - \nu n_{yy})$	4
	$\varepsilon_{yy} = \frac{1}{E\,t}(n_{yy} - \nu n_{xx})$	5
	$\gamma_{xy} = \frac{2(1+\nu)}{E\,t} n_{xy}$	6
equilibrium equations	$\frac{\partial n_{xx}}{\partial x} + \frac{\partial n_{xy}}{\partial y} + k_y(n_{xx} - n_{yy}) + 2k_x n_{xy} + p_x = 0$	7
	$\frac{\partial n_{yy}}{\partial y} + \frac{\partial n_{xy}}{\partial x} + k_x(n_{yy} - n_{xx}) + 2k_y n_{xy} + p_y = 0$	8
	$k_{xx} n_{xx} + 2k_{xy} n_{xy} + k_{yy} n_{yy} + p_z = 0$	9

Membrane forces in a spherical dome

The forces in a spherical dome can be computed by maple using the shell membrane equations (p. 38). The dome is loaded by self-weight *p* only. The result is shown in figure 52. For example, a dome with a radius *a* = 12 m and self-weight *p* = 2 kN/m² will give a hoop force in the bottom edge of $n = p\,a = 2 \times 12 = 24$ kN/m tension.

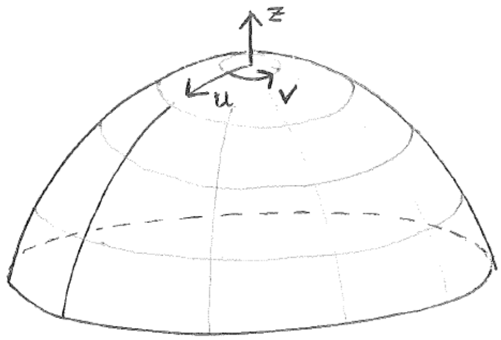

Figure 51. Curved coordinates on a spherical dome

```
> restart:
> kxx:=-1/a: kyy:=-1/a: kxy:=0: ax:=1: ay:=sin(u/a):
> ky:=diff(ay,u)/ax/ay: kx:=diff(ax,v)/ay/ax:
> px:=p*sin(u/a): py:=0: pz:=-p*cos(u/a): # p:=t*rho*g:
> nxx:=f1(u): nyy:=f2(u): nxy:=0:
> eq1:= kxx*nxx + kyy*nyy + 2*kxy*nxy + pz = 0:
> eq2:= diff(nxx,u)/ax + diff(nxy,v)/ay + (nxx-nyy)*ky + 2*nxy*kx + px = 0:
> eq3:= diff(nyy,v)/ay + diff(nxy,u)/ax + (nyy-nxx)*kx + 2*nxy*ky + py = 0:
> dsolve({eq1,eq2});
```

$$\left\{ \mathrm{f1}(xs) = -\frac{2\left(p\cos\left(\frac{xs}{a}\right)a + \_C1\right)}{-1+\cos\left(\frac{2\,xs}{a}\right)}, \mathrm{f2}(xs) = \frac{1}{2}\,\frac{5\,p\cos\left(\frac{xs}{a}\right)a + 4\,\_C1 - p\,a\cos\left(\frac{3\,xs}{a}\right)}{-1+\cos\left(\frac{2\,xs}{a}\right)} \right\}$$

```
> # boudary condition nxx(0)=nyy(0)
> f1:=-2*(p*cos(u/a)*a+_C1)/(-1+cos(2*u/a)):
> f2:=1/2*(5*p*cos(u/a)*a+4*_C1-p*a*cos(3*u/a))/(-1+cos(2*u/a)):
> solve(f1=f2,_C1):
> _C1:=-p*a:
>
> nxx:= -p*a/(1+cos(u/a)):                    # meridional force, pressure line
> nyy:= -p*a*( cos(u/a) - 1/(1+cos(u/a)) ): # hoop force
> nxy:= 0:
> p:=1:       # self-weight [kN/m2]
> a:=10:      # radius [m]
> um:=Pi/2*a: # maximum u value [m]
> f:=-0.3:    # plot factor -
> plot({[ a       *sin(u/a), a       *cos(u/a),u=-um..um],
        [(a+f*nxx)*sin(u/a),(a+f*nxx)*cos(u/a),u=-um..um],
        [(a+f*nyy)*sin(u/a),(a+f*nyy)*cos(u/a),u=-um..um]},
color=[black,red,green],thickness=[3,1,1]);
```

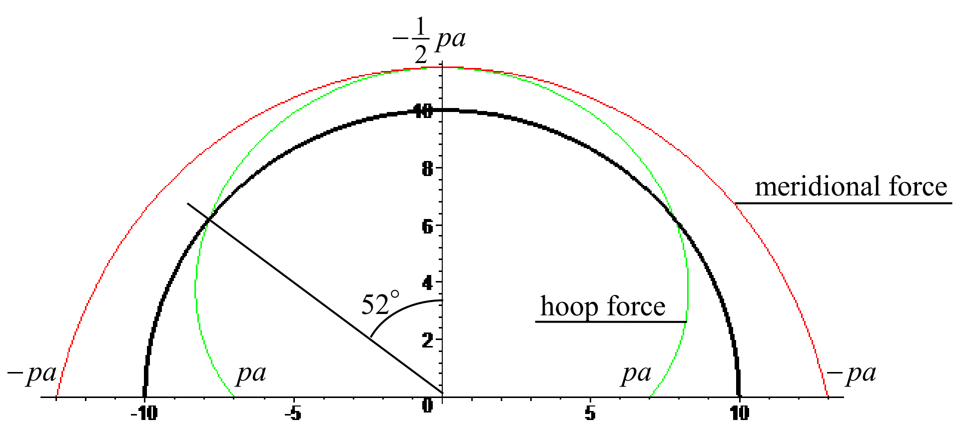

Figure 52. Membrane forces in a spherical dome

Derivation of membrane equation 1

An imaginary fibre in the x direction will elongate with du_x (fig. 53). Strain is elongation over length, therefore,

$$\varepsilon_{xx1} = \frac{du_x}{dx} .$$

The imaginary fibre will shorten due to u_z (fig. 53). The new fibre length is angle times radius

$$\frac{s}{\frac{1}{k_{xx}}} \times \left(\frac{1}{k_{xx}} - u_z\right) = s\,(1 - u_z k_{xx}) ,$$

therefore,

$$\varepsilon_{xx2} = \frac{s - s\,(1 - u_z k_{xx})}{s} = u_z k_{xx} .$$

The imaginary fibre will elongate due to displacement u_y (fig. 53). The fibre strain is

$$\varepsilon_{xx3} = \frac{\frac{s}{r_y}(r_y + u_y) - s}{s} = \frac{u_y}{r_y} = u_y k_x .$$

The total strain is $\varepsilon_{xx} = \varepsilon_{xx1} - \varepsilon_{xx2} + \varepsilon_{xx3} = \frac{\partial u_x}{\partial x} - k_{xx} u_z + k_x u_y$.

Q.E.D.

Shell membrane equation 2 can be derived in the same way.

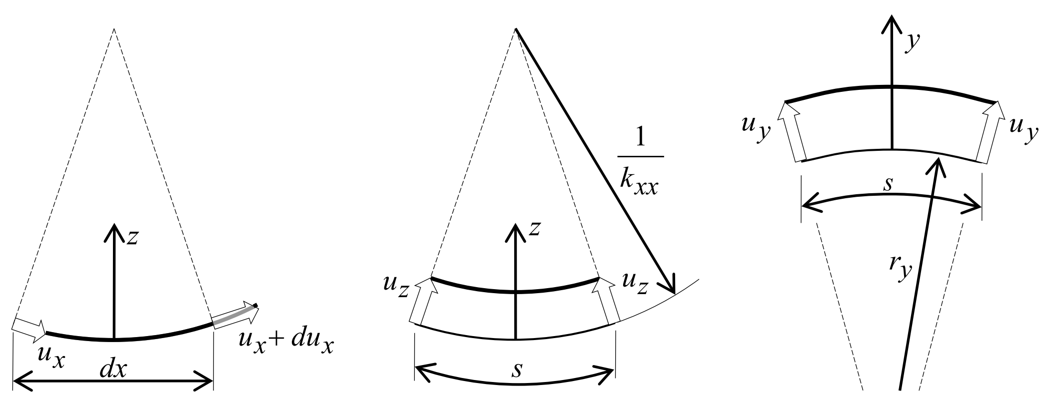

Figure 53. Deformation in the x direction; in the z direction; in the y direction

Derivation of membrane equation 3

The first two terms of equation 3 are the same as for plates (fig. 54).

$$\gamma_{xy,1} = \frac{du_x}{dy} + \frac{du_y}{dx}$$

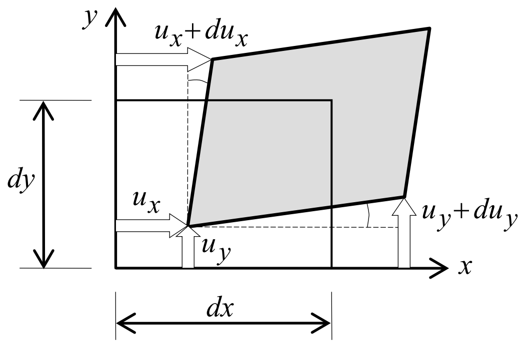

Figure 54. Deformation in the x and y direction

Since u_z is perpendicular to the surface a uniform u_z causes shear in the panel (fig. 55).

$$\gamma_{xy,2} = \frac{u_z \dfrac{k_{xy}\, dx\, dy}{dx}}{dy} + \frac{u_z \dfrac{k_{xy}\, dx\, dy}{dy}}{dx} = 2k_{xy} u_z \,.$$

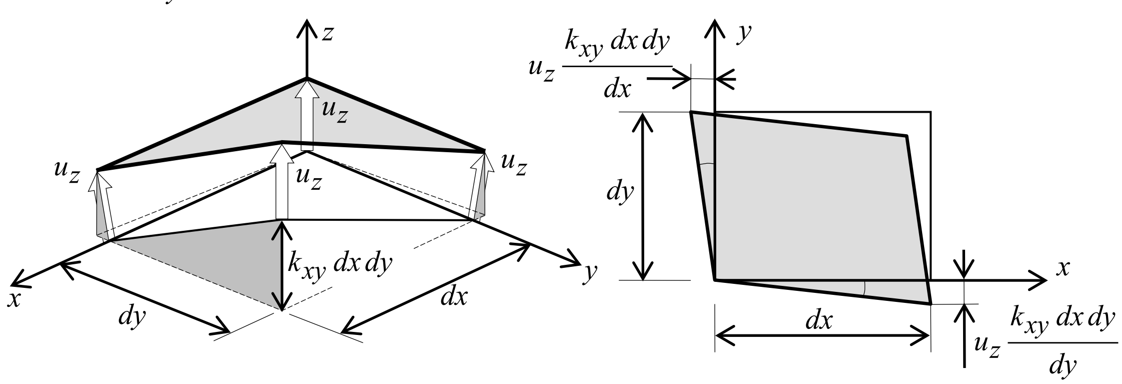

Figure 55. Deformation due to displacement in the z direction

In a curved coordinate system a uniform deformation u_x produces a shear strain (fig. 56).

$$\gamma_{xy3} = k_x u_x$$

In the same way can be derived $\gamma_{xy4} = k_y u_y$.

The total shear deformation is

$$\gamma_{xy} = \gamma_{xy1} - \gamma_{xy2} - \gamma_{xy3} - \gamma_{xy4} = \frac{\partial u_x}{\partial y} + \frac{\partial u_y}{\partial x} - 2k_{xy} u_z - k_x u_x - k_y u_y \,.$$

Q.E.D.

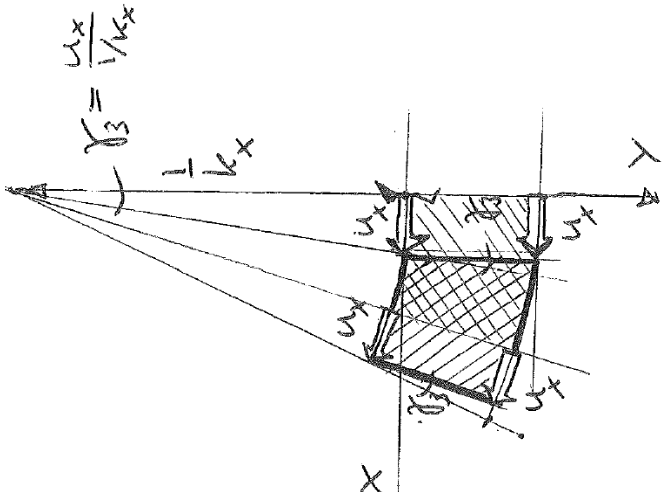

Figure 56. Shear deformation due to uniform x displacement in a curved coordinate system

Duomo di Firenze

The cathedral of Firenze (Florence, Italy) has a dome with a span of 44 m (fig. 57). The builder of the dome was Filippo Brunelleschi. As far as we know he had only two examples, the Pantheon (p. 14) and the *Hagia Sophia*. The Pantheon has a span of 43.4 m and is made of concrete. However, it had been built 1500 years before and the recipe for making concrete had been forgotten. The Hagia Sophia has a span of 31 m and is made of brick. However, it has large buttresses which the people of Firenze thought were ugly. Brunelleschi made a brick design with an inner and an outer shell (fig. 58). Construction of the dome started in 1420 and took 16 years. Many historians see this dome as the end of the middle ages and the start of the renaissance.[3]

Figure 57. Duomo di Firenze, Italy [11]

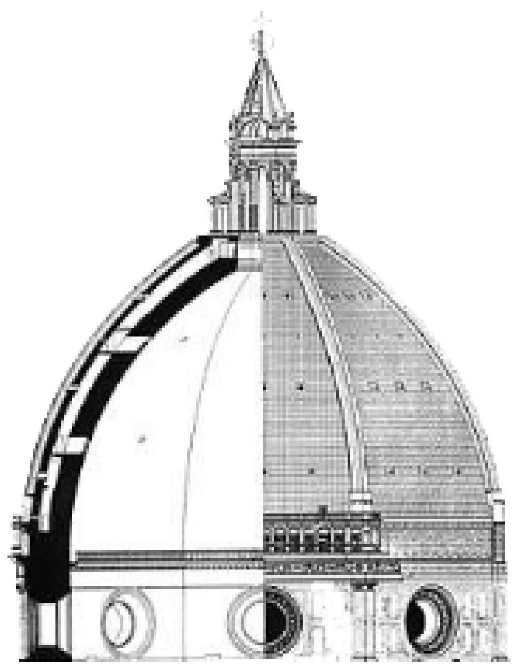

Figure 58. Cross-section of the dome [12]

[3] Time frame: In 1505 Leonardo da Vinci painted his Mona Lisa.

In the lower part of the dome the hoop forces are tension. This is carried by stone blocks connected by iron bars. Without this the dome would crack and collapse. Fortunately, the iron did not corrode away in the more than 570 years that the dome exists. Humidity in the masonry is carefully monitored.

Saint Paul's Cathedral

Saint Paul's cathedral in London was built from 1675 until 1711.[4] The design has been made by Christopher Wren who also supervised construction (see cables and arches p. 5). The outside dome is made of timber (fig. 59, 60). The inside dome is made of bricks and has an oculus. In between is a third dome. This dome is cone shaped and made of bricks. It carries the stone lantern and supports the outside dome. Note that the pressure line (p. 6) in the domes and the cathedral walls is very clear. This designer knew exactly what he was doing. The dome spans approximately 35 m.

Under the dome is the famous whispering gallery. When you are at this gallery and whisper something it can be clearly heard by someone on the other side of the gallery. This is because sound waves are guided along the curved wall of the gallery. Clapping your hands produces no less than four echoes. The name "whispering gallery" is now generally used for this acoustical effect in physics.

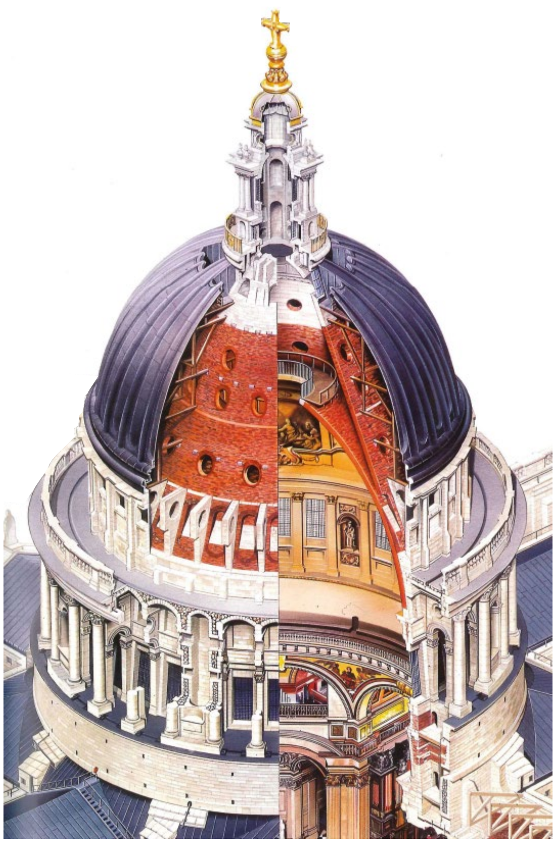

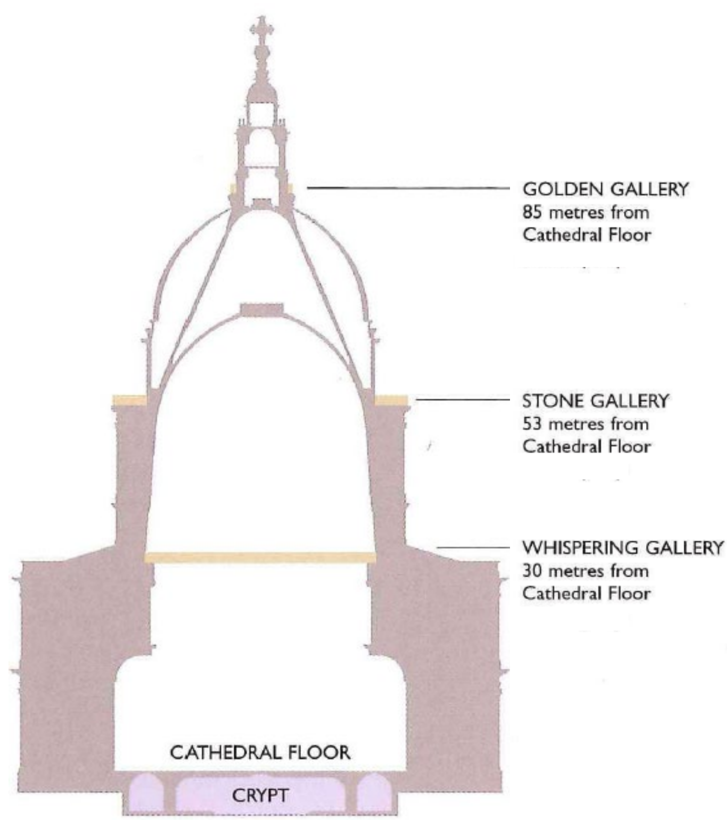

Figure 59. Dome of Saint Paul's cathedral [13] Figure 60. Cross-section of the cathedral [14]

[4] Time frame: In 1684 Isaac Newton discovered the laws of motion, with which we calculate trajectories of objects on earth and in space. In 1765 James Watt invented the steam engine with condenser, which marks the start of the industrial revolution. When you visit Saint Paul's Cathedral you can literally touch the civilization that produced these big steps in human development. As a consequence we speak English today.

Derivation of membrane equation 7

Figure 61 left top shows a small shell part with only normal force n_{xx}. Three forces act on this shell part. Equilibrium in the x direction gives

$$p_{x1}dxdy + (n_{xx} + \frac{\partial n_{xx}}{\partial x}\frac{dx}{2})\vartheta_1(\frac{1}{k_y} + \frac{dx}{2}) - (n_{xx} - \frac{\partial n_{xx}}{\partial x}\frac{dx}{2})\vartheta_1(\frac{1}{k_y} - \frac{dx}{2}) = 0$$

This can be simplified to $\frac{\partial n_{xx}}{\partial x} + k_y n_{xx} + p_{x1} = 0$.

Figure 61 left bottom shows a small shell part with only normal force n_{yy}. Three forces act on this shell part too. Equilibrium in the x direction gives

$$p_{x2}dxdy - n_{yy}dx\vartheta 1 = 0$$

This can be simplified to $-k_y n_{yy} + p_{x2} = 0$.

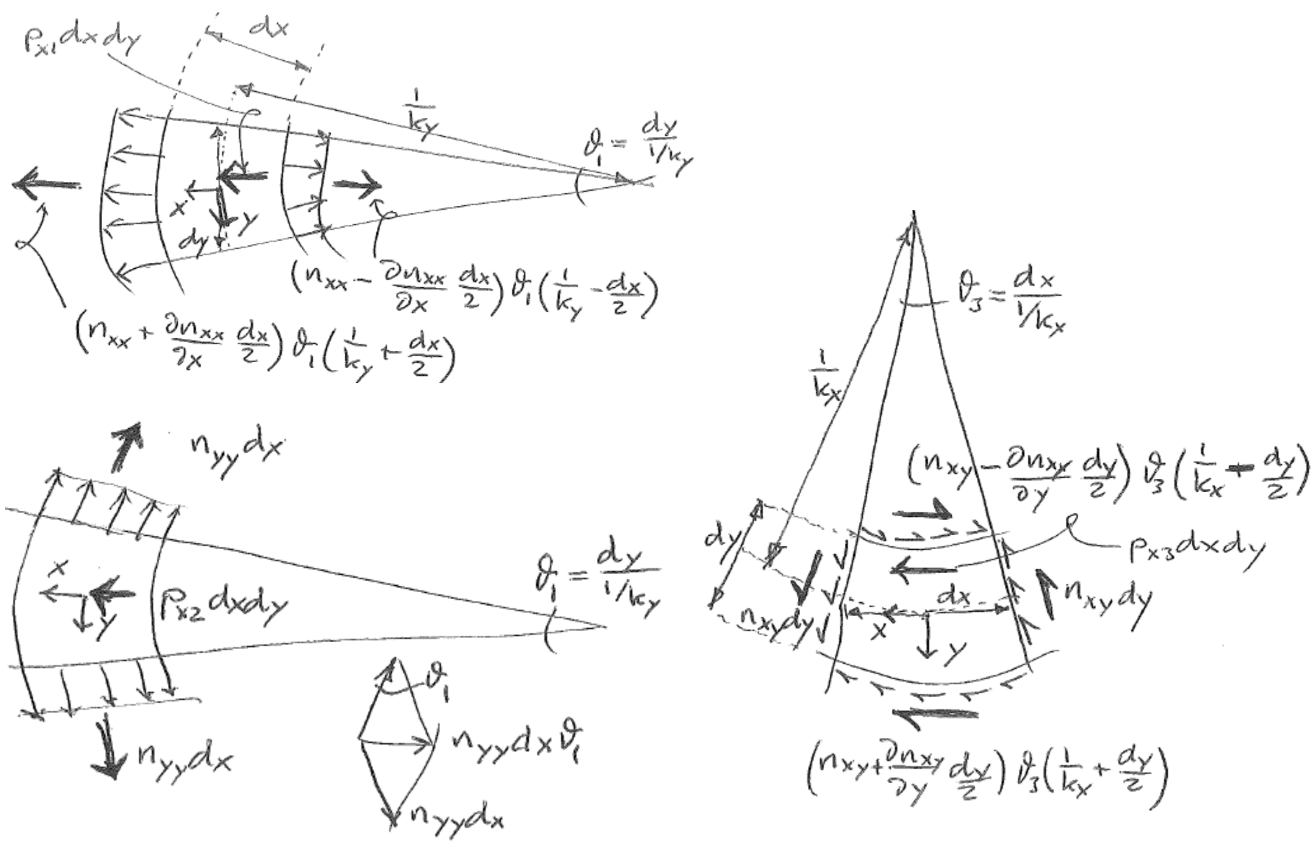

Figure 61. Equilibrium of a curved plate part in the x direction

Figure 61 right shows a small shell part with only shear force n_{xy}. Four forces act on this shell part. Equilibrium in the x direction gives

$$p_{x3}dxdy + (n_{xy} + \frac{\partial n_{xy}}{\partial y}\frac{dy}{2})\vartheta_3(\frac{1}{k_x} + \frac{dy}{2}) - (n_{xy} - \frac{\partial n_{xy}}{\partial y}\frac{dy}{2})\vartheta_3(\frac{1}{k_x} - \frac{dy}{2}) + n_{xy}dy\vartheta_3 = 0$$

This can be simplified to $\frac{\partial n_{xy}}{\partial y} + 2k_x n_{xy} + p_{x3} = 0$.

Substitution in $p_x = p_{x1} + p_{x2} + p_{x3}$ gives

$$\frac{\partial n_{xx}}{\partial x} + \frac{\partial n_{xy}}{\partial y} + k_y(n_{xx} - n_{yy}) + 2k_x n_{xy} + p_x = 0$$

Q.E.D.

Shell membrane equation 8 can be derived in the same way.

Derivation of membrane equation 9
A shell part can be curved in the *x* direction (fig. 62). It needs to be in equilibrium in the *z* direction. This is described by Barlow's formula (p. 8).

$$n_{xx} + p_{z1}\frac{1}{k_{xx}} = 0\,.$$

A shell part that is curved in the *y* direction gives a similar equilibrium equation

$$n_{yy} + p_{z2}\frac{1}{k_{yy}} = 0\,.$$

A shell part can also be twisted (fig. 63). Equilibrium in the *z* direction gives

$$n_{xy}\,dy\frac{k_{xy}dxdy}{dy} + n_{xy}\,dx\frac{k_{xy}dxdy}{dx} + p_{z3}\,dx\,dy = 0\,,$$

which can be simplified to

$$2\,n_{xy}k_{xy} + p_{z3} = 0$$

For a shell part that is curved in all three ways k_{xx}, k_{yy} and k_{xy} the load p_z is obtained by summation.

$$p_{z1} + p_{z2} + p_{z3} = p_z$$

Substitution of the previous four equations gives

$$k_{xx}n_{xx} + k_{yy}n_{yy} + 2k_{xy}n_{xy} + p_z = 0$$

Q.E.D.

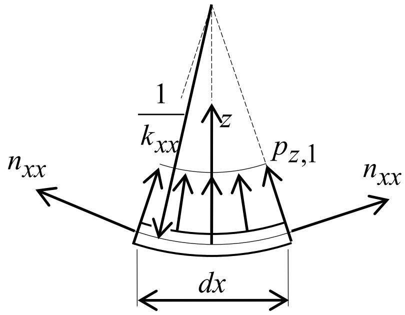

Figure 62. Equilibrium of a curved shell part

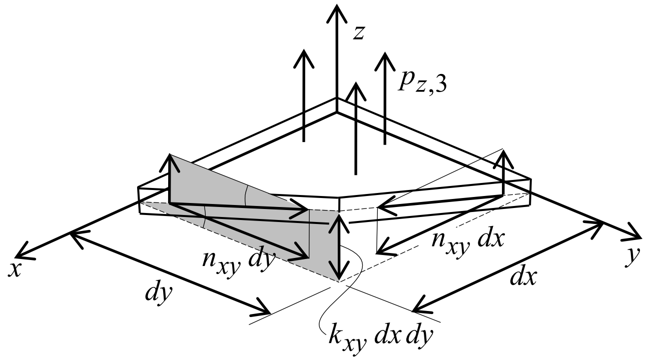

Figure 63. Equilibrium of a twisted shell part

Soap bubbles and soap films

A free soap bubble is a sphere (fig. 64). When a bubble is attached to an object its shape is more difficult to describe. A step in the right direction is that for any bubble the mean curvature k_m (p. 24) is constant over the surface. This is proven here by applying shell membrane equation 9 (p. 38).

Soap has the properties of a liquid; there is no shear stress and the normal stress is the same in all directions. Therefore, $n_{xy} = 0$ and $n_{xx} = n_{yy} = n$. Substitution in equation 1 gives

$$\tfrac{1}{2}(k_{xx} + k_{yy}) = -\frac{p_z}{2n},$$

which is by definition equal to k_m. The air pressure in the bubble is a little larger than outside due to the stress in the soap membrane. The over pressure p_z is the same everywhere in the bubble and the force n is the same everywhere in the membrane. Consequently, the mean curvature is everywhere the same. Q.E.D.

A soap film in a wire loop is free to minimise its area (fig. 65). Therefore, it is called a minimal surface. It has equal air pressure on both sides. Therefore, $p_z = 0$, consequently, $k_m = 0$ everywhere in the film. This property is often used in form finding (p. 16) of tent structures.

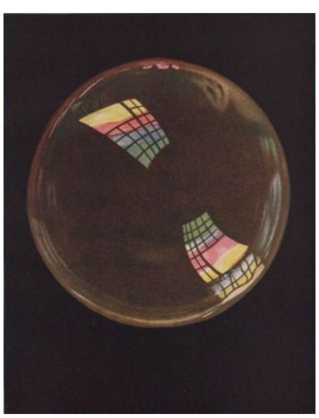
Figure 64. Free soap bubble

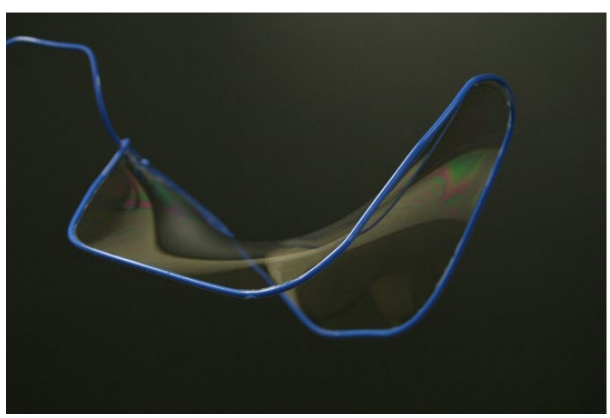
Figure 65. Soap film in a wire loop

Beam calculation of a simply supported tube
Consider a simply supported beam with an evenly distributed load (fig. 66). The cross-section of the beam is circular (fig. 67). The load is self-weight p [kN/m²].

In a handbook we find the moment of inertia $I = \pi a^3 t$.

From figure 67 we derive the distributed line load $q = 2\pi a\, p$ [kN/m].

Elementary mechanics gives us the moment in the middle $M = \frac{1}{8} q l^2$,

the stress at the bottom $\sigma = \dfrac{M\, a}{I}$,

and the deflection in the middle $w = \dfrac{5}{384} \dfrac{q l^4}{EI}$.

Substitution in the last two equations gives $\sigma = \dfrac{p l^2}{4 a t}$ and $w = \dfrac{5}{192} \dfrac{p l^4}{a^2 E t}$.

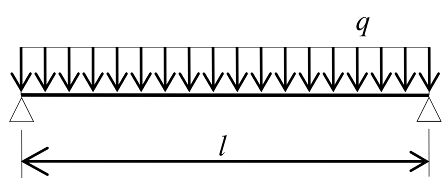

Figure 66. Simply supported beam

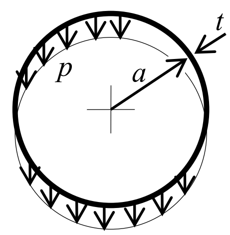

Figure 67. Cross-section of the beam

Shell calculation of a simply supported tube
Consider the simply supported beam (fig. 66). The coordinate system is shown in figure 68. We see that

$$k_{xx} = 0, \quad k_{yy} = -\frac{1}{a}, \quad k_{xy} = 0, \quad \alpha_x = 1, \quad \alpha_y = 1$$

$$p_x = 0, \quad p_y = p \sin\frac{v}{a}, \quad p_z = -p \cos\frac{v}{a}.$$

At both ends $u = \frac{1}{2} l$ and $u = -\frac{1}{2} l$ the tube is closed by a thin diaphragm. This diaphragm can carry membrane forces without buckling but it cannot carry bending moments. The middles of the diaphragms are fixed.

The boundary conditions are

$u = \frac{1}{2} l$	$u_z = 0$	1
	$u_y = 0$	2
	$n_{xx} = 0$	3
$u = 0$	$u_x = 0$	4
	$n_{xy} = 0$	5

Most boundary conditions are obvious. Only boundary condition 5 is explained (fig. 69). The shell and the loading are symmetrical. Symmetry and equilibrium have opposite requirements for the directions of the stresses at $u = 0$. Therefore, the only possible stress is zero stress.

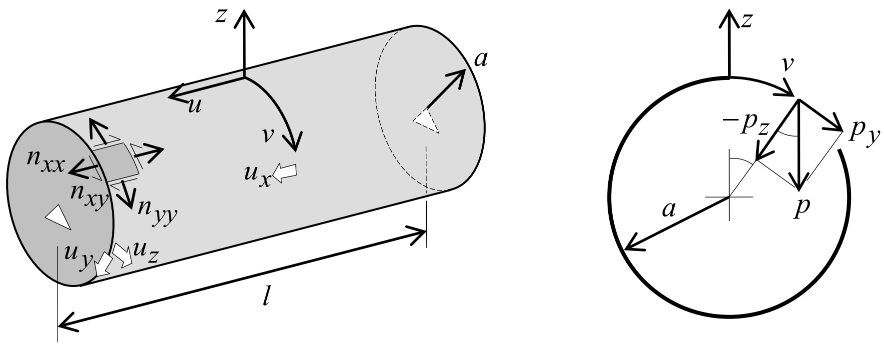

Figure 68. Local coordinate system of the tube

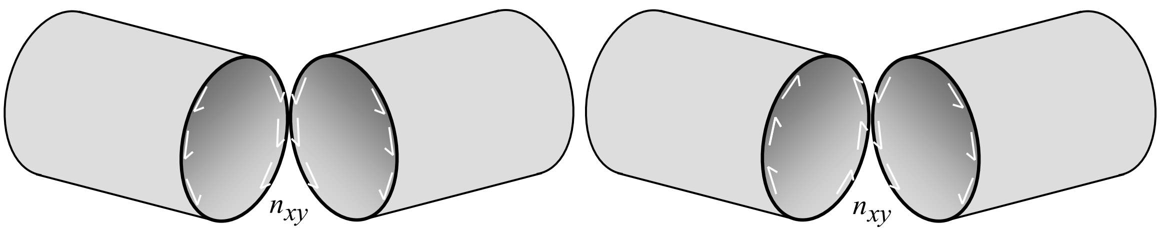

Figure 69. Shear stresses in the middle section due to symmetry (left) and equilibrium (right)

Shell calculation of the stresses

In this section the stresses in the tube are calculated using the shell membrane equations (p. 38).

Equation 9 simplifies to $-\dfrac{n_{yy}}{a} - p\cos\dfrac{v}{a} = 0$ from which we solve $n_{yy} = -p\,a\cos\dfrac{v}{a}$.

Equation 8 simplifies to $p\sin\dfrac{v}{a} + \dfrac{\partial n_{xy}}{\partial x} + p\sin\dfrac{v}{a} = 0$ from which we solve $n_{xy} = -2\,p\,u\sin\dfrac{v}{a} + C_1$.

Boundary condition $n_{xy}(0, v) = 0$ gives $C_1 = 0$.

Equation 7 simplifies to $\dfrac{\partial n_{xx}}{\partial x} - \dfrac{2pu}{a}\cos\dfrac{v}{a} + 0 = 0$ from which we solve $n_{xx} = \dfrac{pu^2}{a}\cos\dfrac{v}{a} + C_2$.

Boundary condition $n_{xx}(\tfrac{1}{2}l, v) = 0$ gives $C_2 = -\dfrac{p(\tfrac{1}{2}l)^2}{a}\cos\dfrac{v}{a}$.

For steel tubes the Von Mises stress (p. 101) in the middle bottom $(u, v) = (0, \pi a)$ is important.

$$n_{VM} = \sqrt{n_{xx}^2 - n_{xx}n_{yy} + n_{yy}^2 + 3n_{xy}^2}$$

Using $\sigma_{VM} = \dfrac{n_{VM}}{t}$, this can be evaluated to $\boxed{\sigma_{VM\,\max} = \dfrac{pl^2}{4at}\sqrt{1 - 4\dfrac{a^2}{l^2} + 16\dfrac{a^4}{l^4}}}$.

We see that for long tubes $(l >> a)$ the shell result is the same as the beam result (see beam calculation p. 47). For a short tube of $l = 6a$ the shell result is 5% smaller than the beam result.

Exercise: What is the stress in the top of the beam?

Statically determinate
In the previous section, the stresses everywhere in the tube are calculated using the equilibrium equations only. Therefore, the tube is a statically determinate structure. This is typical for shell structures:

If the support is statically determinate, than the membrane stresses are statically determinate.[5]

Tube shear stress
The shear force V in the tube cross-section is (fig. 70)

$$V = \int_{v=0}^{2\pi a} n_{xy} \sin\frac{v}{a} dy = -2\pi a\, p u \, .$$

The largest shear stress in the tube cross-sections is

$$\tau_{\max} = \frac{n_{xy}(u, \frac{1}{2}\pi a)}{t} = \frac{-2 p u}{t} \, .$$

Expressed in shear force V and cross-section area A it becomes[8]

$$\boxed{\tau_{\max} = \frac{V}{\frac{1}{2}A}}.$$

Shell calculation of the tube deformation
In this section the deformation of a simply supported tube is calculated using the shell membrane equations (p. 38). The solutions of n_{xx}, n_{yy} and n_{xy} are substituted in equations 4, 5 and 6.

Equation 1 simplifies to $\frac{p}{a E t}\left(u^2 - \frac{1}{4} l^2 + \nu a^2\right)\cos\frac{v}{a} = \frac{\partial u_x}{\partial x}$ from which we solve

$u_x = \frac{p u}{a E t}\left(\frac{1}{3} u^2 - \frac{1}{4} l^2 + \nu a^2\right)\cos\frac{v}{a} + C_3$.

Boundary condition 4 gives $C_3 = 0$.

Equation 3 simplifies to $-\frac{4 p u}{E t}(1+\nu)\sin\frac{v}{a} = -\frac{p u}{a^2 E t}\left(\frac{1}{3} u^2 - \frac{1}{4} l^2 + \nu a^2\right)\sin\frac{v}{a} + \frac{\partial u_y}{\partial x}$ from which

we solve $u_y = \frac{p u^2}{a^2 E t}\left(\frac{1}{12} u^2 - \frac{1}{2} a^2 (4 + 3\nu) - \frac{1}{8} l^2\right)\sin\frac{v}{a} + C_4$

Boundary condition 2 gives $C_4 = \frac{p l^2}{a^2 E t}\left(\frac{5}{192} l^2 + \frac{1}{2} a^2 + \frac{3}{8}\nu a^2\right)\sin\frac{v}{a}$.

[5] Statically determinate is a model property. A more advanced model of the same structure can be statically indetermined.

Eq. 2 simplifies to $\frac{p}{a\,E\,t}\left(-\nu u^2 - a^2 + \frac{1}{4}\nu l^2\right)\cos\frac{v}{a} = \frac{p u^2}{a^3 E\,t}\left(\frac{1}{12}u^2 - \frac{1}{2}a^2(4+3\nu) - \frac{1}{8}l^2\right)\cos\frac{v}{a} +$

$+\frac{p l^2}{a^3 E\,t}\left(\frac{5}{192}l^2 + \frac{1}{2}a^2 + \frac{3}{8}\nu a^2\right)\cos\frac{v}{a} + \frac{u_z}{a}$ from which we solve

$$u_z = \frac{p}{a^2 E\,t}\left(-\frac{1}{12}u^4 + \frac{1}{8}a^2(4u^2 - l^2)(4+\nu) + \frac{1}{8}u^2 l^2 - a^4 - \frac{5}{192}l^4\right)\cos\frac{v}{a}$$

The deflection of the middle bottom $(u, v) = (0, \pi a)$ is important.

$$\boxed{u_{z\,\max} = \frac{p l^4}{a^2 E\,t}\left(\frac{5}{192} + \frac{\nu+4}{8}\frac{a^2}{l^2} + \frac{a^4}{l^4}\right)}$$

For long tubes $(l >> a)$ the shell result is the same as the beam result (see beam calculation of a simply supported tube p. 47). The second term is caused by shear deformation. The last term is caused by ovalization of the cross-section. For a tube of $l = 20a$ the shell result is 5% larger than the beam result. For a short tube of $l = 6a$ the shell result is 61% larger than the beam result.

Bernoulli's hypothesis

Jacob Bernoulli's hypothesis is: *Plane cross-sections remain plane during bending.*[6] It is the starting point for deriving section moments in beams, plates and shells. We can test this hypothesis for tubes using the shell solution.[7] The deformation in the *x* direction is

$$u_x = \frac{p u}{a\,E\,t}\left(\frac{1}{3}u^2 - \frac{1}{4}l^2 + \nu a^2\right)\cos\frac{v}{a}.$$

This can be written as

$$u_x = C\,d\,,$$

where $C = \frac{p u}{a^2\,E\,t}\left(\frac{1}{3}u^2 - \frac{1}{4}l^2 + \nu a^2\right)$ and $d = a\cos\frac{v}{a}$.

Factor *d* is the distance of the considered material point to the neutral axis. It is a function of *v*. Please note the difference between ν (Poisson's ratio) and *v* (curvilinear coordinate). Factor *C* is not a function of *v* and it depends on the considered cross-section. Therefore, u_x is linear in *d* and Bernoulli's hypothesis is true for tubular sections despite the presence of shear forces. For tubular sections it should be called Bernoulli's theorem.[8]

---

[6] Jacob Bernoulli (1654-1705) was a professor of mathematics at the University of Basel in Switzerland.

[7] Note that in this section Bernoulli's hypothesis is applied to a beam with a thin-wall circular cross-section. Here, it is not applied to the thin shell wall.

[8] For other cross-section shapes Bernoulli's hypothesis is not true due to shear and torsion deformation. Fortunately, the linear distribution of normal stresses due to bending – which follows from Bernoulli's hypothesis – is true for all cross-sections of slender beams.

Shear stiffness
Shear stiffness is defined as

$$GA_s = \frac{V}{\gamma},$$

where V is the shear force and γ is the shear deformation of a slice of a beam (fig. 70). For the considered tube we obtain

$$V = \int_{v=0}^{2\pi a} n_{xy} \sin\frac{v}{a} dy = -2\pi a\, p u$$

$$\gamma = \frac{\partial u_y}{\partial x}(u, \tfrac{1}{2}\pi a) + \frac{u_x(u,\pi a) - u_x(u,0)}{2a} = \frac{-4 p u(1+\nu)}{Et}$$

$$\frac{V}{\gamma} = \frac{-2\pi a\, p u}{\frac{-4 p u(1+\nu)}{Et}} = \frac{E}{2(1+\nu)}\frac{1}{2}2\pi a t = \frac{1}{2}GA$$

So,

$$\boxed{GA_s = \frac{1}{2}GA}.$$ [9]

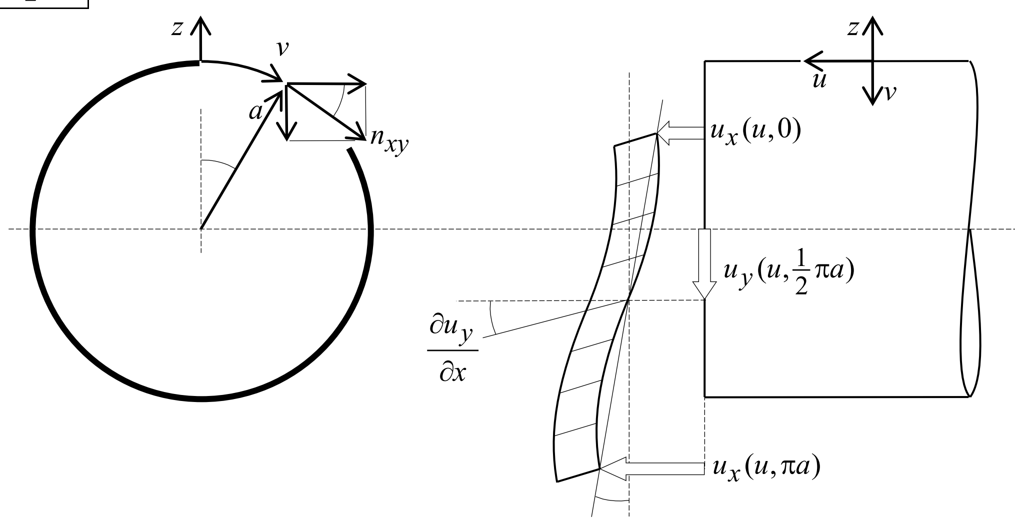

Figure 70. Shear deformation of a tube slice. Bernoulli's hypothesis (p. 50) has not been used.

[9] For thick wall tubes the shear stiffness is $GA_s = (\frac{1}{2} + \frac{3}{4}\frac{t}{a})GA$ and the largest shear stress is $\tau_{\max} = (2 + \frac{t}{a})\frac{V}{A}$. This has been derived from finite element analysis using volume elements [15].

Gap

Boundary condition 1 has not been used. Here it is checked if this boundary condition is fulfilled. The displacement in the radial direction is

$$u_z = \frac{p}{a^2 E t}\left(-\tfrac{1}{12}u^4 + \tfrac{1}{8}a^2(4u^2 - l^2)(4+\nu) + \tfrac{1}{8}u^2 l^2 - a^4 - \tfrac{5}{192}l^4\right)\cos\frac{v}{a}$$

At $u = \pm\frac{1}{2}l$ this simplifies to $u_z = \dfrac{-a^2 p}{E t}\cos\dfrac{v}{a}$ which is not zero.

Therefore, boundary condition 1 is not fulfilled. There is a gap between the diaphragm and the shell (fig. 71). To close the gap the shell needs to bend. This deformation is not part of the membrane equations. To fulfil all boundary conditions the membrane equations need to be extended with bending (see Sanders-Koiter equations p. 54). The phenomenon of strong bending close to edges is called edge disturbance (p. 14, p. 71). It is typical for thin shell structures.

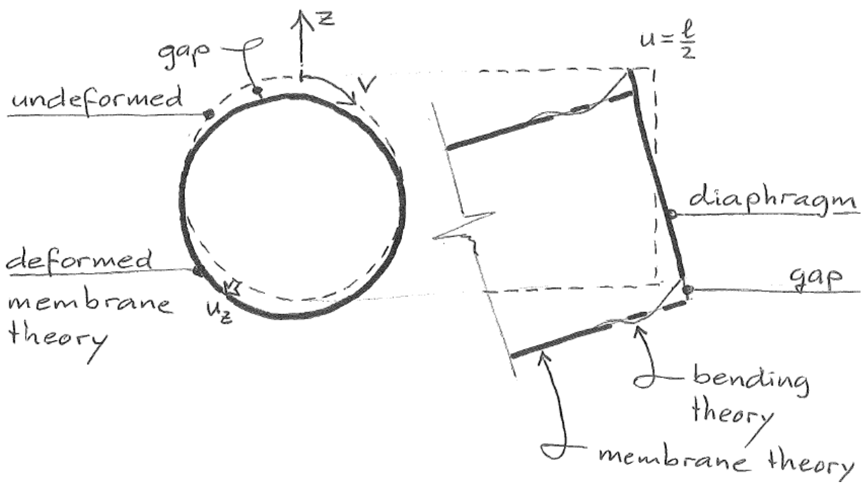

Figure 71. Boundary condition 1 is not fulfilled

Monocoque

The first airplane structures were a frame of wood or steel covered with a skin of cotton fabric. In 1912 a racing plane was built with a skin of three glued layers of wood veneer in total 4 mm thick (fig. 72, 73). This skin was also the load bearing structure, so a frame was not applied. The French company that build these planes was founded by Armand Deperdussin.[10] The plane was called the Deperdussin monocoque (Pronounce mo-no-cock without emphasis. Monos is alone in Greek; coquille is shell in French) [Wikipedia]. To us it looks like a normal plane but in those days its shape was different from any other plane, for example, it had one set of main wings instead of two above each other. The plane won several races and set the world speed record. Ever since, the word monocoque is used for structures that are fast and derive a large part of their strength from their skin. Examples are racing cars, rockets and army tanks.

[10] Armand Deperdussin (1860–1924) was a French business man [Wikipedia].

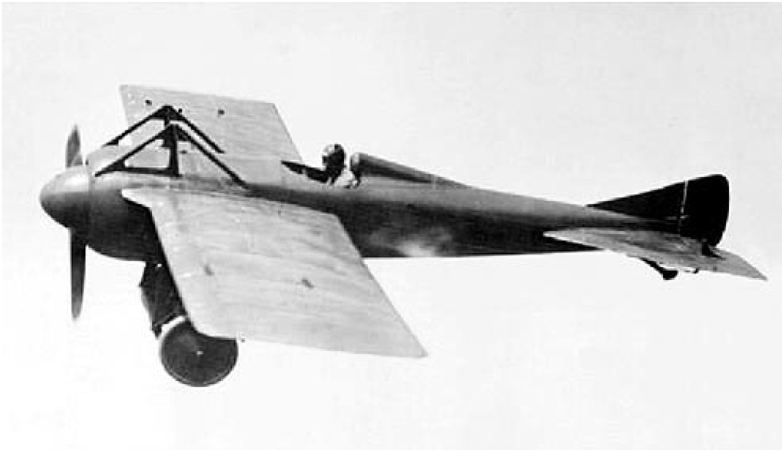

Figure 72. Deperdussin monocoque airplane [photo 1913 Musée de l'Air et de l'Space, Paris]

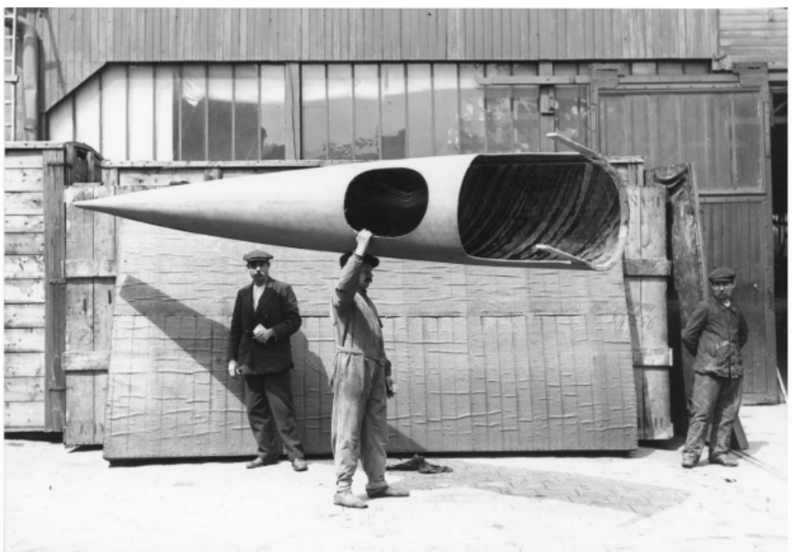

Figure 73. Fuselage of the Deperdussin monocoque
[photo G. Printamp 1912, Smithsonian's National Air and Space Museum, Washington]

Structural models overview
In scientific literature often the following names are used for structural idealisations.

structural element	name	deformation included
beams	Euler-Bernoulli beam	bending
	Timoshenko beam	bending and shear
plates loaded in plane	Navier equations	extension
plates loaded perpendicularly to their plane	Kirchhoff plate	bending
	Reissner-Mindlin plate (p. 61)	bending and shear
	Von Kármán-Föppl equations	extension, bending and large displacements
shells	Shell membrane equations (p. 38)	extension
	Sanders-Koiter equations (p. 54)	extension and bending
	several theories	extension, bending and shear

Shell theory

In 1888 Augustus Love[11] formulated the basic equations that govern the behaviour of thin elastic shells [18, 19]. He used Jacob Bernoulli's[12] hypothesis, which was also used by Gustav Kirchhoff [13] in formulating the plate theory. In the years that followed there was much discussion on this shell theory. Some inconsistencies were found. Many scientists proposed other equations, such as Wilhelm Flügge[14] (1934) [20], Ralph Byrne[15] (1944) [21], Eric Reissner[16] (1952) [22] and Paul Naghdi[17] (1957) [23]. Also Love himself proposed improved equations [24]. Lyell Sanders[18] was the first to remove all inconsistencies from Love's first equations [25]. Independently, Warner Koiter[19] proved that Love's initial assumptions were correct after all and he also derived the correct shell equations [26, 27]. In 1959 there was a conference in the aula of Delft University where Sanders presented the correct shell equations and Koiter presented the correct shell equations. One of Koiter's papers on the subject has the clear title "All you need is Love." [28].

Love's first equations are called the first approximation theory. Including improvements they are referred to as the Sanders-Koiter equations (p. 54). Other theories account for out-of-plane shear deformation and are called higher-order approximation theory. They are intended for thick shells (p. 13).

Before 1959, equations were developed for specific shell shapes. For example, equations for cylindrical shells were proposed by Lloyd Donnell[20] (1934) [29] and Leslie Morley[21] (1959) [30].

Sanders-Koiter equations

The following 21 equations describe membrane action and bending action in thin shell structures. Equation 18 is derived below (p. 66). The other equations are not derived in these notes but they can be obtained in the same way. The derivation of Sanders and that of Koiter can be found in literature [25] and [26, 27] respectively. The derivation of Koiter is based on tensor analysis and is most rigorous. The equations are valid for elastic material behaviour and small displacements. They correctly predict no stresses for rigid translations. The equations do not change when the local coordinate system is rotated around the z axis. The equations correctly produce symmetrical stiffness matrices (Betti's reciprocal theorem). The Sanders-Koiter equations include the equations for plates. In other words, with appropriate values for $k_{xx}, k_{yy}, k_{xy}, \alpha_x, \alpha_y$ the Sanders-Koiter equations simplify to the equations for plates loaded in plane, plates loaded perpendicular to their plane (Kirchhoff theory), circular plates and the shell membrane equations

[11] Augustus Love (1863–1940) was a mathematician and professor in Oxford [Wikipedia].
[12] Jacob Bernoulli (1654–1705) was a professor of mathematics in Bazel [Wikipedia].
[13] Gustav Kirchhoff (1824–1887) was a German physicist and professor in Berlin, Breslau and Heidelberg. He is also well-known in physics for discoveries such as Kirchhoff's laws on electrical current [Wikipedia].
[14] Wilhelm Flügge (1904–1990) was professor of civil engineering in Göttingen. After the second world war he and his wife moved to the USA and became professors in Stanford [Wikipedia].
[15] Ralph Byrne (1912–1948) was associate professor of applied mechanics in Caltech, Pasadena. [31,32]
[16] Eric Reissner (1913–1996) was professor of applied mechanics in MIT and San Diego. His father, Hans Reißner (1874–1967) was an aircraft engineer and professor in Aachen and Berlin. The family moved from Berlin to the Illinois just before the second world war [Wikipedia].
[17] Paul Naghdi (1924–1994) was born in Tehran. He studied in the USA and became professor of mechanical engineering in Berkeley [Wikipedia].
[18] Lyell Sanders (1924–1998) was professor of structural mechanics in Harvard [German Wikipedia].
[19] Warner Koiter (1914–1997) was professor of applied mechanics in Delft [Wikipedia].
[20] Lloyd Donnell (1895–1997) was professor of mechanical engineering in Illinois [Wikipedia].
[21] Leslie Morley (1924–2011) was a scientist in the Royal Aircraft Establishment and a professor in Brunel University, London [Wikipedia].

(p. 38). This is clearly a remarkable achievement of the 20th century scientists. The Sanders-Koiter equations are a scientific masterpiece. [22]

Table 4. Sanders-Koiter equations

kinematic equations	$\varepsilon_{xx} = \dfrac{\partial u_x}{\partial x} - k_{xx}u_z + k_x u_y$	1
	$\varepsilon_{yy} = \dfrac{\partial u_y}{\partial y} - k_{yy}u_z + k_y u_x$	2
	$\gamma_{xy} = \dfrac{\partial u_x}{\partial y} + \dfrac{\partial u_y}{\partial x} - 2k_{xy}u_z - k_x u_x - k_y u_y$	3
	$\varphi_x = -\dfrac{\partial u_z}{\partial x} - k_{xx}u_x - k_{xy}u_y$	4
	$\varphi_y = -\dfrac{\partial u_z}{\partial y} - k_{yy}u_y - k_{xy}u_x$	5
	$\varphi_z = \frac{1}{2}(-\dfrac{\partial u_x}{\partial y} + \dfrac{\partial u_y}{\partial x} - k_x u_x + k_y u_y)$	6
	$\kappa_{xx} = \dfrac{\partial \varphi_x}{\partial x} - k_{xy}\varphi_z + k_x \varphi_y$	7
	$\kappa_{yy} = \dfrac{\partial \varphi_y}{\partial y} + k_{xy}\varphi_z + k_y \varphi_x$	8
	$\rho_{xy} = \dfrac{\partial \varphi_x}{\partial y} + \dfrac{\partial \varphi_y}{\partial x} + (k_{xx} - k_{yy})\varphi_z - k_x\varphi_x - k_y\varphi_y$	9
constitutive equations	$n_{xx} = \dfrac{Et}{1-\nu^2}(\varepsilon_{xx} + \nu\varepsilon_{yy})$	10
	$n_{yy} = \dfrac{Et}{1-\nu^2}(\varepsilon_{yy} + \nu\varepsilon_{xx})$	11
	$\dfrac{n_{xy} + n_{yx}}{2} = \dfrac{Et}{2(1+\nu)}\gamma_{xy}$	12
	$m_{xx} = \dfrac{Et^3}{12(1-\nu^2)}(\kappa_{xx} + \nu\kappa_{yy})$	13
	$m_{yy} = \dfrac{Et^3}{12(1-\nu^2)}(\kappa_{yy} + \nu\kappa_{xx})$	14

[22] The following dates provide a time frame. In 1822, Claude-Louis Navier formulated the Navier-Stokes equations which describe the behaviour of fluids [Wikipedia]. In 1850, Gustav Kirchhoff completed the differential equation that describes the behaviour of plates [Wikipedia]. In 1865, James Clerk-Maxwell unified many laws into Maxwell's equations that describe electric and magnetic fields [Wikipedia]. In 1916, Albert Einstein found the Einstein field equations describing the structure of the universe [Wikipedia]. In 1925 and 1926, Werner Heisenberg, Max Born and Pascual Jordan found the Heisenberg equation of quantum mechanics describing materials on a very small scale [Wikipedia].

	$m_{xy} = \dfrac{Et^3}{24(1+\nu)}\rho_{xy}$	15
equilibrium equations	$v_x = \dfrac{\partial m_{xx}}{\partial x} + \dfrac{\partial m_{xy}}{\partial y} + k_y(m_{xx} - m_{yy}) + 2k_x m_{xy}$	16
	$v_y = \dfrac{\partial m_{yy}}{\partial y} + \dfrac{\partial m_{xy}}{\partial x} + k_x(m_{yy} - m_{xx}) + 2k_y m_{xy}$	17
	$n_{xy} - n_{yx} = -k_{xy}(m_{xx} - m_{yy}) + (k_{xx} - k_{yy})m_{xy}$	18
	$p_x = -\dfrac{\partial n_{xx}}{\partial x} - \dfrac{\partial n_{yx}}{\partial y} - k_y(n_{xx} - n_{yy}) - k_x(n_{xy} + n_{yx}) + k_{xx}v_x + k_{xy}v_y$	19
	$p_y = -\dfrac{\partial n_{yy}}{\partial y} - \dfrac{\partial n_{xy}}{\partial x} - k_x(n_{yy} - n_{xx}) - k_y(n_{xy} + n_{yx}) + k_{yy}v_y + k_{xy}v_x$	20
	$p_z = -k_{xx}n_{xx} - k_{xy}(n_{xy} + n_{yx}) - k_{yy}n_{yy} - \dfrac{\partial v_x}{\partial x} - \dfrac{\partial v_y}{\partial y} - k_y v_x - k_x v_y$	21

Ping pong ball

Consider a sphere that is deformed into an ellipsoid (fig. 74). Think of a ping pong ball that is squeezed by your hand. The code below shows the evaluation of the Sanders-Koiter equations (p. 56) by Maple. The deformation $u_z = b\cos\dfrac{2u}{a}$, $u_x = 0.49b\sin\dfrac{2u}{a}$ has been obtained by trial and error to minimize the load p_x. The code produces figure 75. Displacement u_y and distributed force p_y are zero and p_x is almost zero. Only p_z is needed to obtain this deformation.

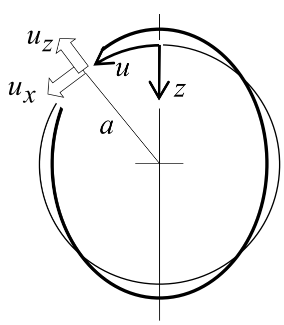

Figure 74. Deformation of a spherical ping pong ball into a prolate ellipsoid shape

```
> a:=20: t:=0.4: E:=1400: nu:=0.3: b:=1:
> kxx:=-1/a: kyy:=-1/a: kxy:=0: alphax:=1: alphay:=sin(u/a):
> ux:=-0.49*b*sin(2*u/a): uy:=0: uz:=b*cos(2*u/a):
>
> ky:=diff(alphay,u)/alphay/alphax: kx:=diff(alphax,v)/alphax/alphay:
> epsilonxx:=diff(ux,u)/alphax-kxx*uz+kx*uy:
> epsilonyy:=diff(uy,v)/alphay-kyy*uz+ky*ux:
> gammaxy:=diff(ux,v)/alphay+diff(uy,u)/alphax-2*kxy*uz-kx*ux-ky*uy:
> phix:=-diff(uz,u)/alphax-kxx*ux-kxy*uy:
> phiy:=-diff(uz,v)/alphay-kyy*uy-kxy*ux:
> phiz:=1/2*(-diff(ux,v)/alphay+diff(uy,u)/alphax-kx*ux+ky*uy):
> kappaxx:=diff(phix,u)/alphax-kxy*phiz+kx*phiy:
> kappayy:=diff(phiy,v)/alphay+kxy*phiz+ky*phix:
> rhoxy:=diff(phix,v)/alphay+diff(phiy,u)/alphax+(kxx-kyy)*phiz-kx*phix-ky*phiy:
```

```
> nxx:=E*t/(1-nu^2)*(epsilonxx+nu*epsilonyy):
> nyy:=E*t/(1-nu^2)*(epsilonyy+nu*epsilonxx):
> nxym:=E*t/(2*(1+nu))*gammaxy:
> mxx:=E*t^3/(12*(1-nu^2))*(kappaxx+nu*kappayy):
> myy:=E*t^3/(12*(1-nu^2))*(kappayy+nu*kappaxx):
> mxy:=E*t^3/(24*(1+nu))*rhoxy:
> vx:=diff(mxx,u)/alphax+diff(mxy,v)/alphay+ky*(mxx-myy)+2*kx*mxy:
> vy:=diff(myy,v)/alphay+diff(mxy,u)/alphax+kx*(myy-mxx)+2*ky*mxy:
> tmp:=kxy*(mxx-myy)-(kxx-kyy)*mxy:
> nxy:=nxym-tmp/2:
> nyx:=nxym+tmp/2:
> px:=-(diff(nxx,u)/alphax+diff(nyx,v)/alphay+ky*(nxx-nyy)+kx*(nxy+nyx)-kxx*vx-kxy*vy):
> py:=-(diff(nyy,v)/alphay+diff(nxy,u)/alphax+kx*(nyy-nxx)+ky*(nxy+nyx)-kyy*vy-kxy*vx):
> pz:=-(kxx*nxx+kxy*(nxy+nyx)+kyy*nyy+diff(vx,u)/alphax+diff(vy,v)/alphay+ky*vx+kx*vy):
>
> plot({ux,uy,uz,px/1.5,py/1.5,pz/1.5},u=0..Pi*a-1);
```

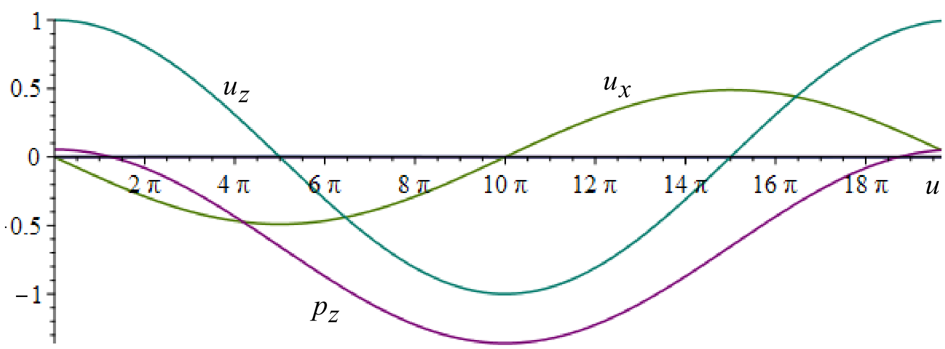

Figure 75. Loading p_z and deformation u_x, u_z of a ping pong ball computed by Maple

Compatibility equation

Sanders-Koiter equations 1 to 9 (p. 54) can be combined resulting in the following equation.

$$-\frac{\partial^2 \varepsilon_{xx}}{\partial y^2} + \frac{\partial^2 \gamma_{xy}}{\partial x \partial y} - \frac{\partial^2 \varepsilon_{yy}}{\partial x^2} = -k_{yy}\kappa_{xx} + k_{xy}\rho_{xy} - k_{xx}\kappa_{yy}$$

In the derivation is used that k_x, k_y and k_G are small (appendix 4.). This equation shows that the strains of the middle surface are connected to the bending deformation. So, we cannot randomly choose functions for the strains ε_{xx}, γ_{xy}, ε_{yy} and randomly choose functions for bending curvatures κ_{xx}, ρ_{xy}, κ_{yy} and expect this could happen in a specific shell with curvatures k_{xx}, k_{xy}, k_{yy}. Therefore, this equation is called the *compatibility equation*. See Shell behaving like a plate (p. 114).

Rigid translation

The Sanders-Koiter equations (p. 54) are accurate for small displacements. However, for large rigid translations they are accurate too. For example, consider a reinforced concrete industrial chimney with a height of 70 m, a radius a = 2.6 m and a wall thickness t = 0.1 m. During a storm the chimney top moves b = 1.0 m which is not exceptional for a chimney of this height.

A rigid translation of the whole chimney (fig. 76) can be described exactly by the displacements

$$u_x = 0, \quad u_y = b\cos\frac{v}{a}, \quad u_z = b\sin\frac{v}{a} \ .$$

Obviously, this translation should not produce strains.

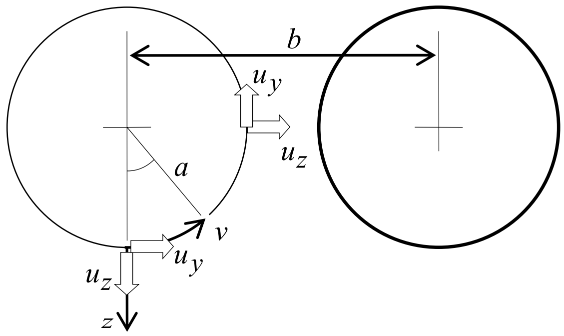

Figure 76. Rigid translation of a cylinder cross-section

From the chimney geometry it follows that $k_{xx} = 0, \quad k_{yy} = -\frac{1}{a}, \quad k_{xy} = 0, \quad \alpha_x = 1, \quad \alpha_y = 1$.

Substitution of these in the kinematic equations 1 to 9 gives

$$\varepsilon_{xx} = 0, \quad \varepsilon_{yy} = 0, \quad \gamma_{xy} = 0, \quad \kappa_{xx} = 0, \quad \kappa_{yy} = 0, \quad \rho_{xy} = 0,$$

which is the correct result. Consequently, the large deflection of the chimney top can be described by the Sanders-Koiter equations.

Exercise: Large rigid rotations do produce unrealistic strains and stresses. Check the Sanders-Koiter equations for this.

Shell differential equations

When the Sanders-Koiter equations (p. 54) are substituted into each other, the following two coupled partial differential equations are obtained (assuming $p_x = p_y = 0$ and v_x, v_y, $n_{xy} - n_{yx}$ are small).

$$-\Gamma\phi + \frac{E t^3}{12(1-\nu^2)} \nabla^2\nabla^2 u_z = p_z$$

and

$$\nabla^2\nabla^2\phi + E t \Gamma u_z = 0,$$

where,

$$\Gamma(.) = k_{xx}\frac{\partial^2(.)}{\partial y^2} - 2k_{xy}\frac{\partial^2(.)}{\partial x \partial y} + k_{yy}\frac{\partial^2(.)}{\partial x^2},$$

$$\nabla^2(.) = \frac{\partial^2(.)}{\partial x^2} + \frac{\partial^2(.)}{\partial y^2} .$$

ϕ is the Airy stress function,[23] which is related to the membrane forces

$$n_{xx} = \frac{\partial^2 \phi}{\partial y^2}, \qquad n_{yy} = \frac{\partial^2 \phi}{\partial x^2}, \qquad n_{xy} = n_{yx} = -\frac{\partial^2 \phi}{\partial x \partial y}.$$

Differential equation type
Linear partial differential equations of the second order are subdivided in three types; elliptic, parabolic and hyperbolic [Wikipedia]. Physicists use this to predict the nature of the solution and select a solution method. The membrane part of the shell differential equations (p. 58) is

$$-\Gamma\phi = p_z$$

In a well-designed thin shell, this part dominates the behaviour. It can be shown that the type of this differential equation depends on the Gaussian curvature k_G (p. 23).

$k_G > 0 \quad \Rightarrow$ elliptic, the solution is local
$k_G = 0 \quad \Rightarrow$ parabolic, the solution extends along one straight line
$k_G < 0 \quad \Rightarrow$ hyperbolic, the solution extends along two straight lines, which are called *characteristics*

Shallow shell differential equation
For cylinders and spheres k_{xx}, k_{yy}, k_{xy} are uniform. This reduces the shell differential equations (p. 58) to

$$\frac{E t^3}{12(1-\nu^2)} \nabla^2\nabla^2\nabla^2\nabla^2 u_z + E t \Gamma\Gamma u_z = \nabla^2\nabla^2 p_z .$$

This is a linear eight order partial differential equation in curvilinear coordinates *u* and *v* (p. 31).

A *shallow shell* is a shell with a sagitta (p. 1) that is small compared to its span. For such shells the curvatures do not change much over the surface and the above differential equation can be a good approximation.

Plate boundary conditions
In general, the solution to an eight order partial differential equation has 8 constants in the *u* direction and 8 constants in the *v* direction. The constants can be solved by 4 boundary conditions on each edge. Figure 77 shows the boundary conditions of a canopy that is fixed on one edge. Note that there are too many boundary conditions. So, some boundary conditions cannot be fulfilled.

This problem also occurs in plates. It was solved by Gustav Kirchhoff [3] in 1850 [34]. He derived the correct boundary conditions of plates from virtual work. Others interpreted his solution as that the stresses due to the torsion moment m_{xy} go round in the edge (fig. 78-1). Therefore, m_{xy} on the edge needs be replaced by a *concentrated shear force V* in the edge (fig. 78-2).

$$m_{xy} dx = V dx \quad \Rightarrow \quad \boxed{V = m_{xy}}$$

[23] George Airy (1801–1892) was an astronomy professor in Cambridge, England [Wikipedia]

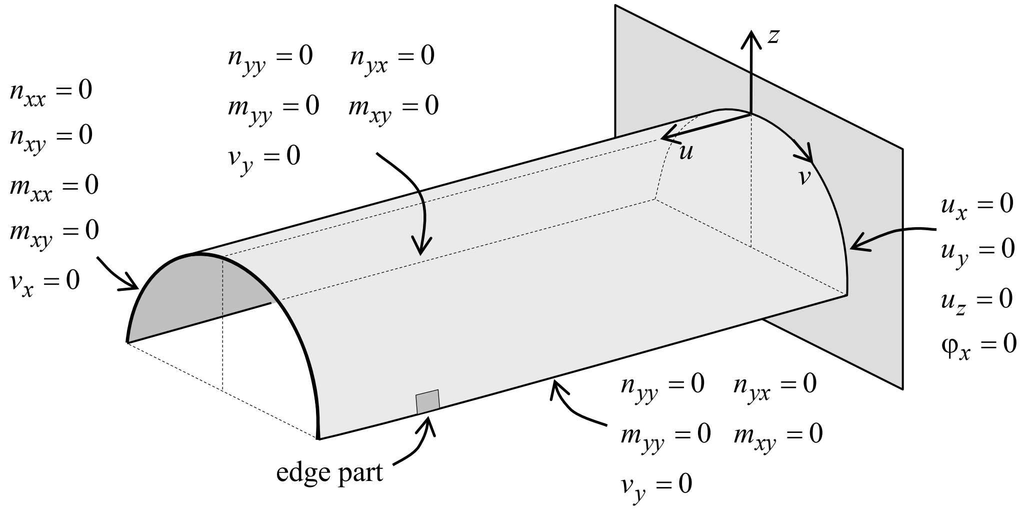

Figure 77. Boundary conditions of a canopy

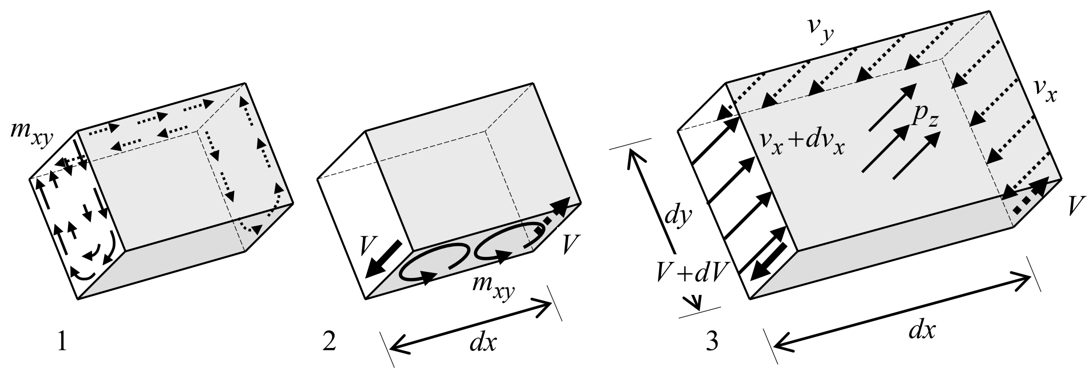

Figure 78. Forces on an edge part

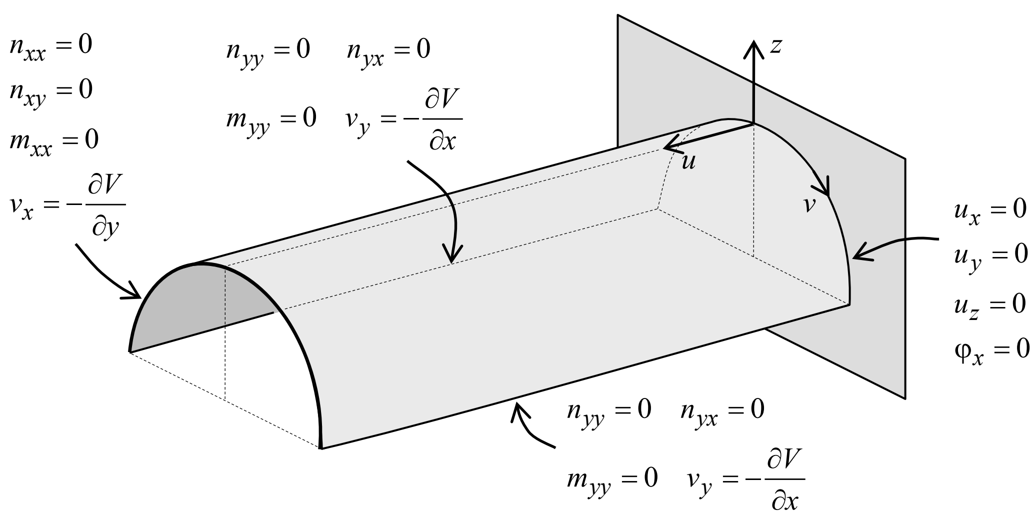

Figure 79. Boundary conditions according to Kirchhoff (plates)

From equilibrium of a somewhat larger edge part (fig. 78-3) it follows that

$$p_z dx dy - v_y dx + (v_x + dv_x) dy - (V + dV) + V - v_x dy = 0 .$$

This can be simplified to

$$p_z dy - v_y + \frac{dv_x}{dx} dy - \frac{dV}{dx} = 0 .$$

When $dy \downarrow 0$ then $-v_y - \frac{dV}{dx} = 0$ which can be written as

$$v_y = -\frac{\partial V}{\partial x} .$$

Now we have 4 boundary conditions per edge and the differential equation can be solved (fig. 79).

Thus, according to Kirchhoff, m_{xy} need not be zero on a plate or shell edge in the *x* or *y* direction. Also v_x need not be zero on an edge in the *y* direction, and v_y need not be zero on an edge in the *x* direction. Clearly, in reality they are zero.

We need to interpret m_{xy} *on an edge as a concentrated shear force V in the edge.*

We need to interpret v on an edge as a change in the concentrated shear force V.

However, the plate boundary conditions are not entirely correct for shells (see shell boundary conditions p. 67).

Exercise: In plates $m_{xy} = 0$ in a fixed edge along the *x* or *y* direction. In shells this can be observed too, however, there are exceptions. Can we show this with the Sanders-Koiter equations?

Reissner-Mindlin plate theory[24]

It is possible to come up with a new shell theory that does not have interpretation problems of the boundary conditions? In fact, the *Reissner-Mindlin theory* [34] for thick plates predicts m_{xy}, v_x and v_y on edges realistically without interpretations (fig. 77). However, to compute these values accurately we need to use very small finite elements on the edges. For example, when a plate is 180 mm thick we need to use finite elements that are less than 20 mm wide. This is impractical due to large computation time and therefore almost never applied. A practical element for a 180 mm plate is more than 250 mm wide. For this mesh m_{xy} will not be zero on the edges also not when the Reissner-Mindlin theory is used. Therefore, also in the Reissner-Mindlin theory we need to interpret the torsion moment on an edge as a concentrated shear force in the edge.

---

[24] The name of this theory refers to Eric Reissner and Raymond Mindlin. Eric Reissner (1913–1996) was a professor of applied mechanics at MIT and the University of California San Diego [Wikipedia]. Raymond Mindlin (1906–1987) was a professor of applied science at Columbia University, USA [Wikipedia]. From our point of view they were very skilled in mathematics. They had to be because they did not have computers.

Edge shear stresses
The shear stress in a plate edge or shell edge is [25]

$$\sigma_{xz} = \frac{3}{2}\frac{v_x}{t} - \frac{3}{2}\sqrt{10}\,\frac{V}{t^2}\,.$$

The formula is valid when the local x axis points in the direction of the edge and the local y axis points outwards (fig. 80). Unfortunately, finite element programs using shell elements do not compute this stress. If important, we need to calculate and check this stress by hand.

The concentrated shear force produces a local stress peak. In many structures a local stress peak is not important because the stress will redistribute (steel yields, reinforced concrete cracks). However, a stress peak is important for materials that do not yield such as glass. A stress peak is also important for fatigue.

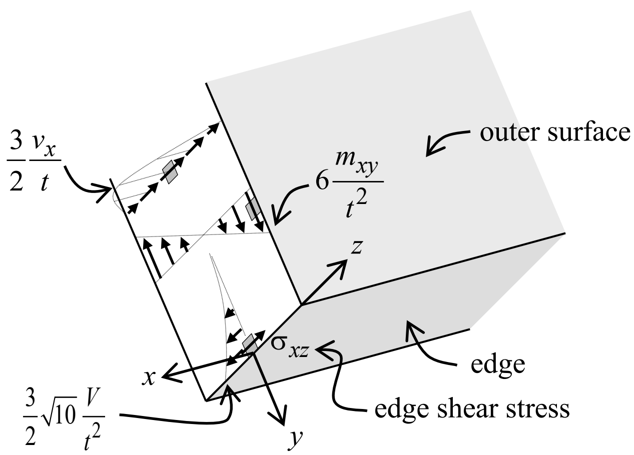

Figure 80. Shear stresses in a free shell edge

Reinforced concrete plate edges
In reinforced concrete plates it is common practice to put hairpins in the edges (fig. 81). A hairpin is a reinforcing bar that is bend in the shape of a U. The hairpins have the same diameter and spacing as the bars perpendicular to the edge. There is a good reason for these hairpins. They carry the concentrated shear force (fig. 82).

[25] In 2010, Johan Blaauwendraad (professor of structural mechanics at Delft University) used Reissner's plate theory (p. 61) to derive the stresses in plate edges. He showed that the shear stress distribution is exponential and the factor of the peak stress is $\frac{3}{2}\sqrt{10}$ [34]. In 2013, Rutger Zwennis (at that time a student at Delft University) modelled a plate loaded in torsion using volume finite elements [35]. He showed that the peak stress due to V includes the factor 4.48 instead of $\frac{3}{2}\sqrt{10} = 4.74$. Who is right? The Reissner plate theory is not exact because Reissner made several assumptions in the derivation. The finite element analyses is not exact either because the number of elements is restricted. In these notes the safe choice of $\frac{3}{2}\sqrt{10}$ has been made. Future computers will be able to determine the factor very accurately.

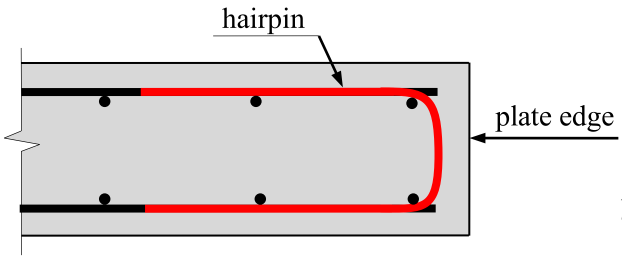

Figure 81. Reinforcement in a cross-section of a concrete plate edge

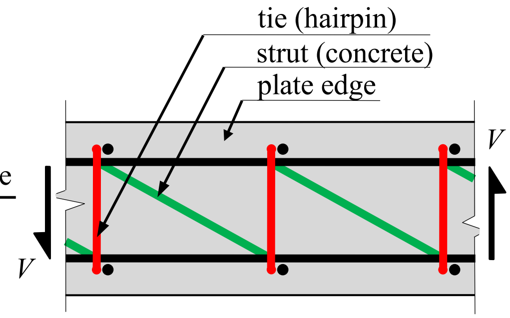

Figure 82. Strut-and-tie model of a reinforced concrete plate edge

Edges that are not in the *x* or *y* direction
If an edge is not in the x direction or y direction, the shear force v_x and the torsion moment m_{xy} need to be transformed to the edge direction. For this we need to rotate the local coordinate systems of the edge finite elements such that one of the axes is in the direction of the edge. The obtained concentrated shear force on a free or simply supported edge can be easily checked because it is equal to $V = \pm\sqrt{m_{xy}^2 - m_{xx}m_{yy}}$, where m_{xy}, m_{xx} and m_{yy} are the moments before rotation.

Proof: Plate moments are a tensor (p. 97). m_1 and m_2 are the principal values (p. 98). The product $m_1 m_2$ is an invariant (p. 23) of this tensor. Therefore, $m_1 m_2 = m_{xx}m_{yy} - m_{xy}^2 = m_{ss}m_{tt} - m_{st}^2$. Suppose that the s axis is perpendicular to the shell edge. Since the edge is free or simply supported $m_{ss} = 0$. Therefore, $m_{xx}m_{yy} - m_{xy}^2 = -m_{st}^2 = -V^2$. Q.E.D.

Palazzetto dello sport [36]
The palazzetto dello sport was built for the 1960 summer Olympics in Rome (fig. 1). It hosted basketball. Nowadays, it is a sports and community centre.
The buttresses are made of prefab concrete. The shell and ribs are made of reinforced concrete that was cast in situ. The formwork of the shell consisted of 1620 cassettes supported by steel tube scaffolding. The cassettes were made of 25 mm thick ferrocement (fig. 83). Ferrocement is a thin layer of mortar with a steel wire mesh inside.

Construction sequence of the dome	*Completed*
- Placing the buttresses - Building the scaffolding for the cassettes. The scaffolding included circular rings made of curved rails of an old railway track. These rings were horizontally elevated onto temporary columns of steel tubes.	
- Building a timber template of a large part of the shell internal surface - Drawing the grid onto the template	August 1956
- Fabrication of moulds for the cassettes. First, onto the timber template the inside shape of one cassette was made of bricks and plaster (fig. 84). Second, a cassette was made onto this inside shape. Third, this cassette was moved down and several moulds were made of this cassette. Etc. - Prefabrication of 30 cassettes a day - Placing the cassettes onto the scaffolding (fig. 85, 86)	December 1956

- Placing reinforcing bars in and on the cassettes - Pouring concrete (fig. 87)	February 1957

architect: Annibale Vitellozzi (1903-1990)
engineer: Pier Luigi Nervi (1891-1979)
contractor: Bartoli

Computer analyses were not performed. Structural calculations were done by hand and checked by scale model tests.

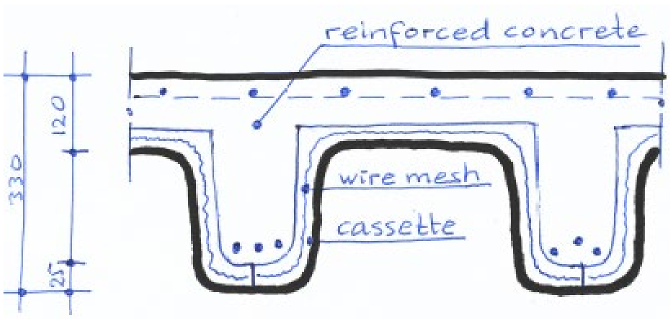

Figure 83. Cross-section of the shell and ribs

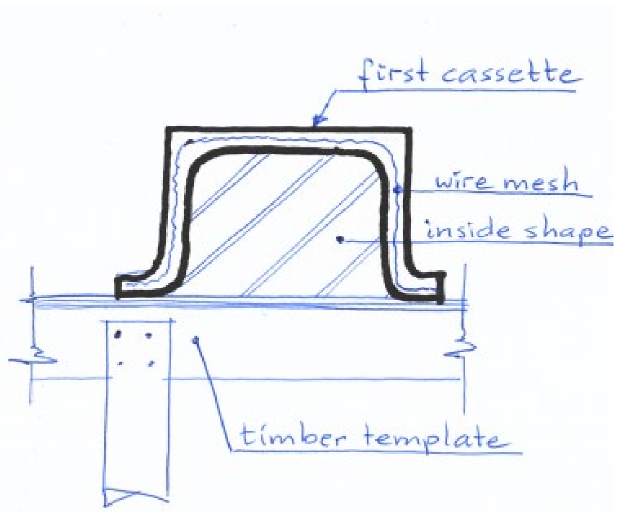

Figure 84. Mould fabrication

Figure 85. A cassette [37]

Figure 86. Scaffolding and cassettes [38]

Figure 87. Construction site during concrete pouring [39]

$n_{xy} \neq n_{yx}$

Sanders and Koiter independently derived that for shells $n_{xy} \neq n_{yx}$. This is a very strange result because shear stresses on perpendicular faces of an infinitesimal cube have the same magnitude $\sigma_{xy} = \sigma_{yx}$ (fig. 88). If the shear stresses are the same, the shear membrane forces must be the same. Nevertheless, Sanders and Koiter are right. This strange results follows from moment equilibrium around the *z* axis of an elementary shell part (see derivation of equation 18 p. 66). It can also be seen in the definition of membrane forces for thick shells in appendix 7.

Finite element programs plot the mean membrane shear force $\frac{1}{2}(n_{xy} + n_{yx})$. It would be interesting to plot the quantity $\frac{1}{2}(n_{xy} - n_{yx})$ too, however, finite element programs do not have this option. It can be shown that $\frac{1}{2}(n_{xy} - n_{yx})$ does not change when the local coordinate system rotates around the z axis (it is an invariant). When $\frac{1}{2}(n_{xy} - n_{yx})$ is large compared to $\frac{1}{2}(n_{xy} + n_{yx})$ then the shell is very thick and should be modelled by volume elements instead of shell elements (see shell thickness p. 13).

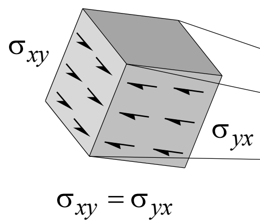

Figure 88. Shear stresses on a small cube

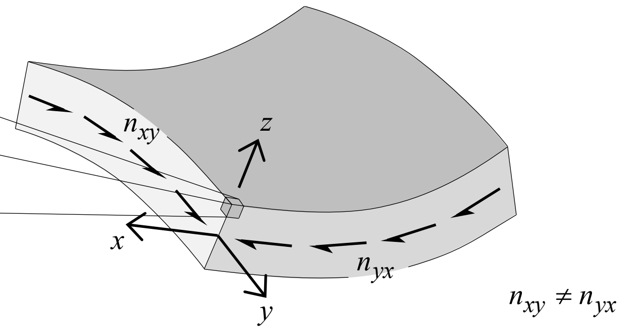

Figure 89. In plane shear forces on a shell part

Challenge: The tensor $\begin{bmatrix} n_{xx} & n_{xy} \\ n_{yx} & n_{yy} \end{bmatrix}$ is not symmetrical. Are the principal directions perpendicular? In what situation are the principal values complex numbers?

Derivation of equation 18

In this note the eighteenth Sanders-Koiter equation (p. 54) is derived. Consider moment equilibrium of a small shell part around the z axis (fig. 90). When the part is only twisted, the bending moments can produce a resulting moment around the z axis.

$$M_{z1} = m_{xx}\, dy\ k_{xy}\, dx - m_{yy}\, dx\ k_{xy}\, dy$$

When the part is curved but not twisted the torsion moment can produce a resulting moment around the z axis.

$$M_{z2} = m_{xy}\, dx\ k_{yy}\, dy - m_{xy}\, dy\ k_{xx}\, dx$$

The in plane shear forces can also produce a moment around the z axis.

$$M_{z3} = n_{xy}\, dy\, dx - n_{yx}\, dx\, dy$$

The total moment around the z axis must be zero.

$$M_{z1} + M_{z2} + M_{z3} = 0$$

This evaluates to

$$k_{xy}(m_{xx} - m_{yy}) - (k_{xx} - k_{yy})m_{xy} + n_{xy} - n_{yx} = 0\,.$$

Q.E.D.

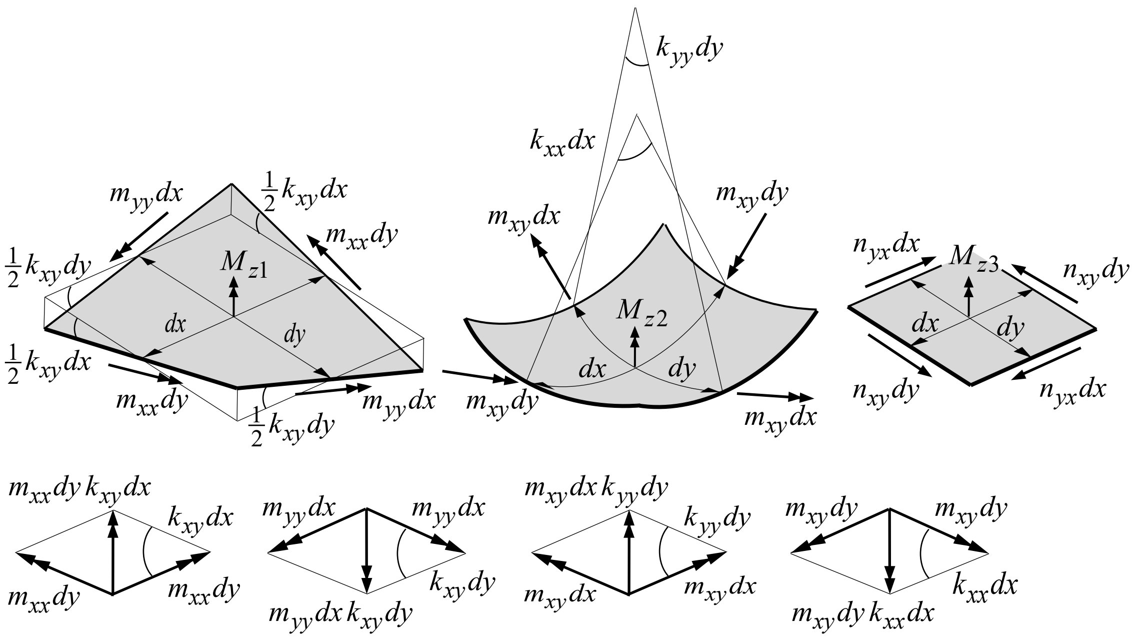

Figure 90. Moment equilibrium around the z axis

Shell boundary conditions

The plate boundary conditions (p. 59) are not completely correct for shells. A shell edge has 3 displacements and 1 rotation. If a value is imposed to one of these a support reaction occurs. Table 5 shows the formulas for computing the support reactions. They are derived from equilibrium of small edge parts (fig. 91 and 92). The table is valid for an edge in the x direction and the y axis pointing outwards. Clearly, instead of imposing a displacement, a distributed edge load can be applied. The table can also be used for formulating these boundary conditions.

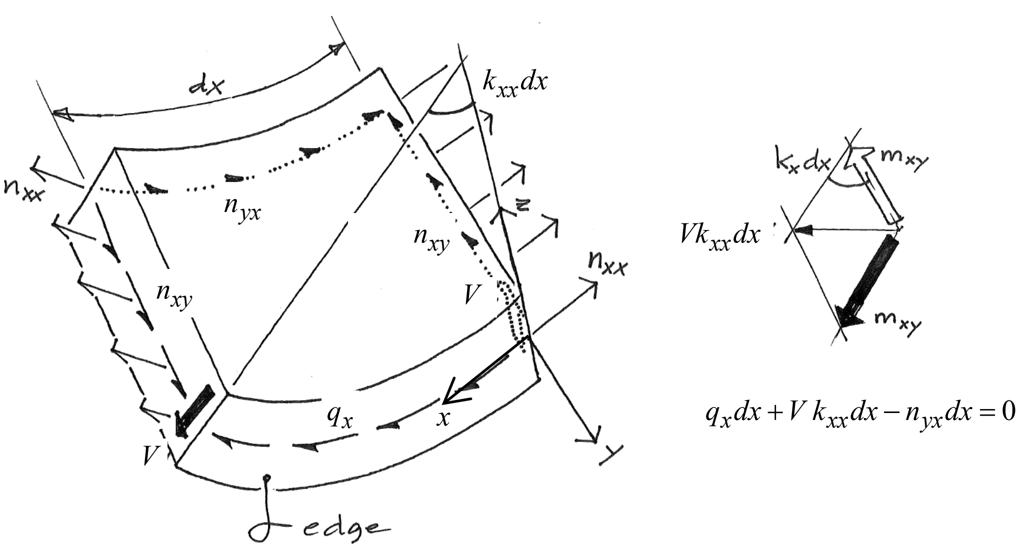

Figure 91. Equilibrium of a shell edge loaded by a distributed shear force q_x

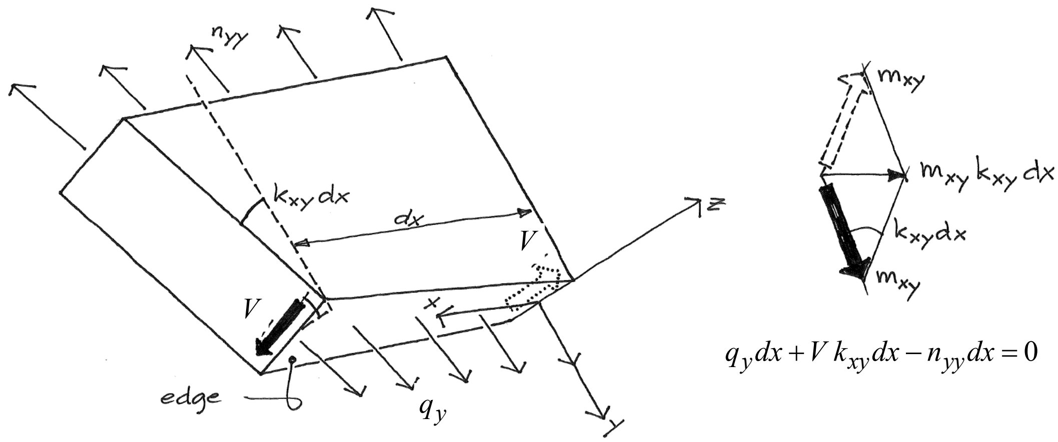

Figure 92. Equilibrium of a shell edge loaded by a distributed normal force q_y

Table 5. Boundary conditions for an edge in the x direction and the y axis pointing outwards

Kinematic (K)		Dynamic (D)		
Impose displacement	u_x	or apply line load	$q_x = n_{yx} - k_{xx}V$.	1
Impose displacement	u_y	or apply line load	$q_y = n_{yy} - k_{xy}V$.	2
Impose displacement	u_z	or apply line load	$q_z = v_y + \dfrac{\partial V}{\partial x}$.	3
Impose rotation	$-\varphi_y$	or apply line moment	$-m_{yy}$.	4

Table 6. Boundary conditions for an edge in the x direction and the y axis pointing inwards

Impose displacement	u_x	or apply line load	$q_x = -n_{yx} + k_{xx}V$.	5
Impose displacement	u_y	or apply line load	$q_y = -n_{yy} + k_{xy}V$.	6
Impose displacement	u_z	or apply line load	$q_z = -v_y - \dfrac{\partial V}{\partial x}$.	7
Impose rotation	$-\varphi_y$	or apply line moment	m_{yy} .	8

Table 7. Boundary conditions for an edge in the y direction and the x axis pointing outwards

Impose displacement	u_x	or apply line load	$q_x = n_{xx} - k_{xy}V$.	9
Impose displacement	u_y	or apply line load	$q_y = n_{xy} - k_{yy}V$.	10
Impose displacement	u_z	or apply line load	$q_z = v_x + \dfrac{\partial V}{\partial y}$.	11
Impose rotation	φ_x	or apply line moment	m_{xx} .	12

Table 8. Boundary conditions for an edge in the y direction and the x axis pointing inwards

Impose displacement	u_x	or apply line load	$q_x = -n_{xx} + k_{xy}V$.	13
Impose displacement	u_y	or apply line load	$q_y = -n_{xy} + k_{yy}V$.	14
Impose displacement	u_z	or apply line load	$q_z = -v_x - \dfrac{\partial V}{\partial y}$.	15
Impose rotation	φ_x	or apply line moment	$-m_{xx}$.	16

Exercise: Proof that $m_{xy} = 0$ in a free corner.

Canopy example, shell boundary conditions

The canopy in figure 93 has curvatures $k_{xx} = k_{xy} = 0,\ k_{yy} = -\frac{1}{a}$. Substitution of these curvatures in the shell boundary conditions (p. 67) gives the canopy boundary conditions.

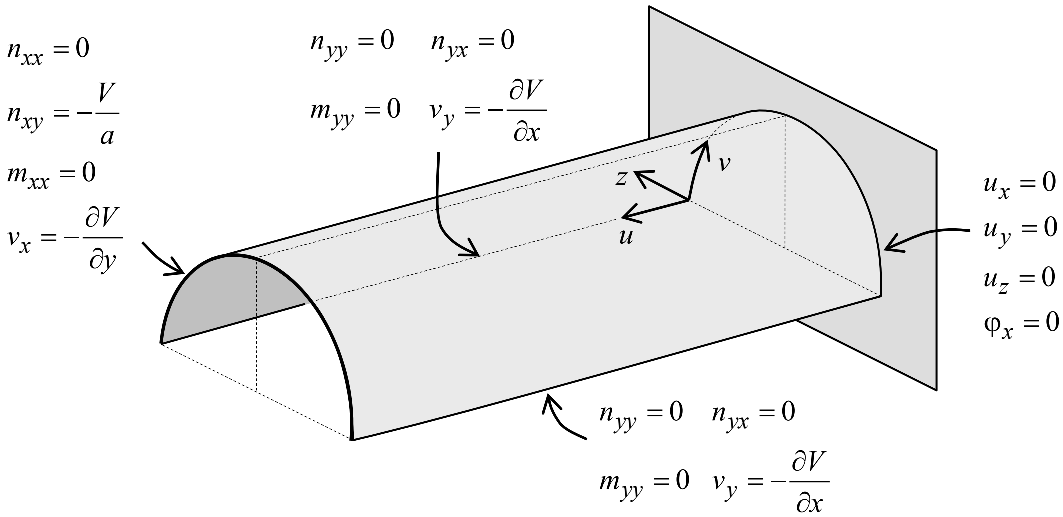

Figure 93. Shell boundary conditions of the canopy

Diaphragm boundary condition

A tube is often closed by a thin wall, called *diaphragm* (fig. 94). The diaphragm can be bend easily out of its plane but it resists deformation in its plane. Therefore, the diaphragm prevents displacement of the tube edge perpendicular to the tube. It also prevents displacement of the tube edge in the direction of the edge. The other displacements are free. This is called a *diaphragm boundary condition*. It is often applied in shell analysis. (Examples on p. 47 and p. 163)

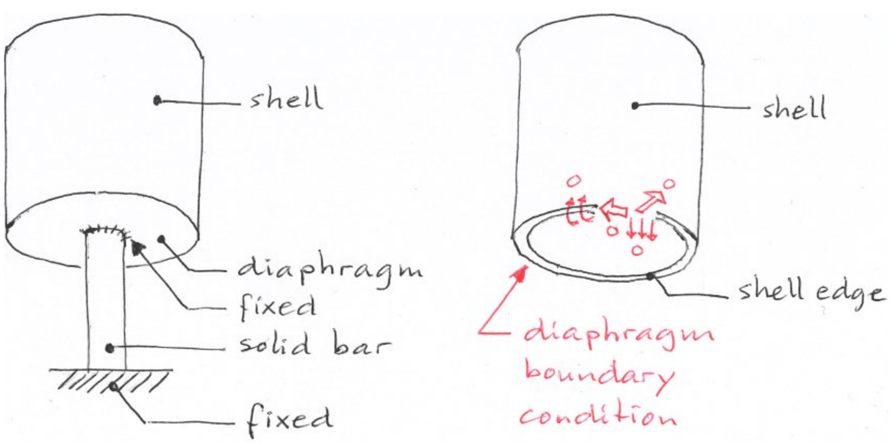

Figure 94. The diaphragm boundary condition can replace a diaphragm.

Edge in the y direction	Edge in the x direction
$n_{xx} - k_{xy}V = 0$	$u_x = 0$
$u_y = 0$	$n_{yy} - k_{xy}V = 0$
$u_z = 0$	$u_z = 0$
$m_{xx} = 0$	$m_{yy} = 0$

Overview of the shell variables

The table below gives an overview of the variables in the Sanders-Koiter equations (p. 54). The variables that need solving are green. They are called *dependent variables*. Note that there are 21 dependent variables and 21 Sanders-Koiter equations. Boundary conditions (p. 67) are imposed on the red edges.

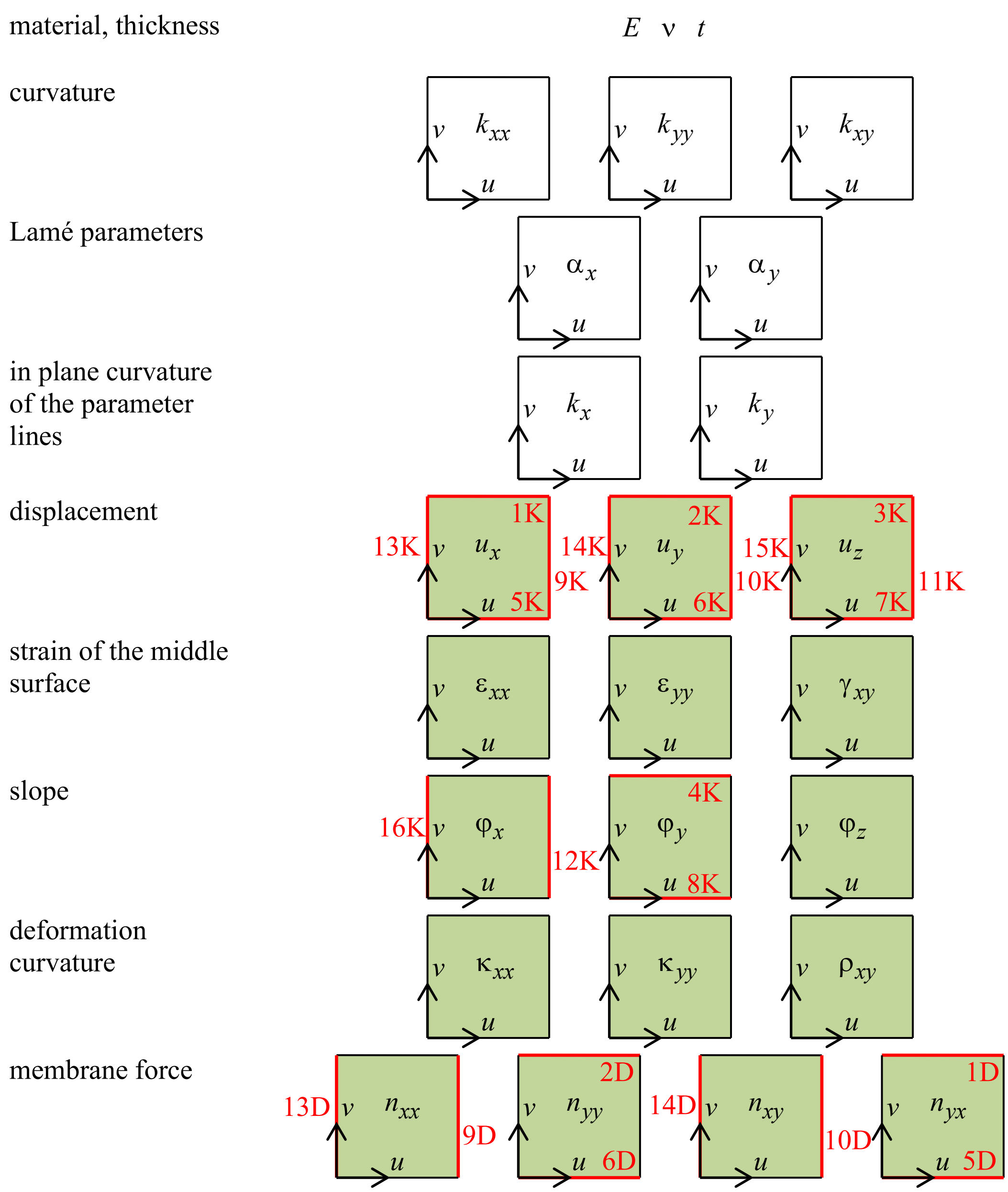

moment

shear force,
out of plane

load

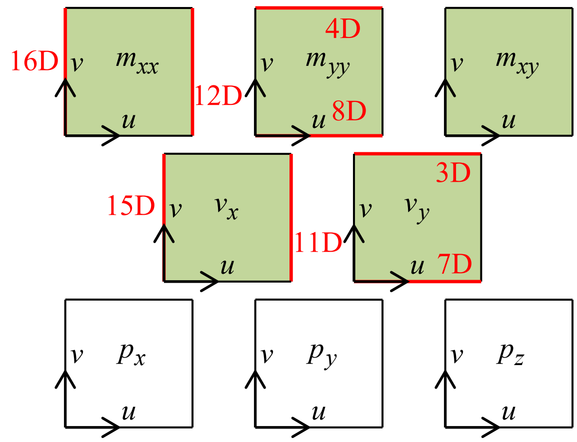

Generalised edge disturbance
An edge disturbance is a large moment at a discontinuity in a shell. This moment is local and at some distance of the discontinuity it is much smaller. Examples of discontinuities are

- Fixed edge or pinned edge
- Point load or line load
- Discontinuity in the distributed load
- Discontinuity in the derivative of the distributed load
- Discontinuity in the middle surface
- Discontinuity in the slope of the middle surface (C_0 continuity p. 11)
- Discontinuity in the curvature of the middle surface (C_1 continuity)
- Change in sign of the Gaussian curvature (p. 23, see differential equation type p. 59)
- Discontinuity in the material stiffness
- Discontinuity in the shell thickness

Exercise: Which of the above discontinuities occur in a torus?

Beam supported by springs
A long beam is supported by uniformly distributed springs (fig. 95). The bending stiffness of the beam is *EI* [Nm²]. The stiffness of the distributed springs is *k* [N/m²]. The differential equation that describes this beam is

$$EI \frac{d^4 w}{dx^4} + k\, w = 0\,.$$

At the left beam end a displacement is imposed and the slope is zero. The right beam end is far away. The boundary conditions are

$$\text{if} \quad x = 0 \quad \text{then} \quad w = w_0 \quad \text{and} \quad \frac{\partial w}{\partial x} = 0$$

$$\text{if} \quad x \to \infty \quad \text{then} \quad w = 0 \quad \text{and} \quad \frac{\partial w}{\partial x} = 0$$

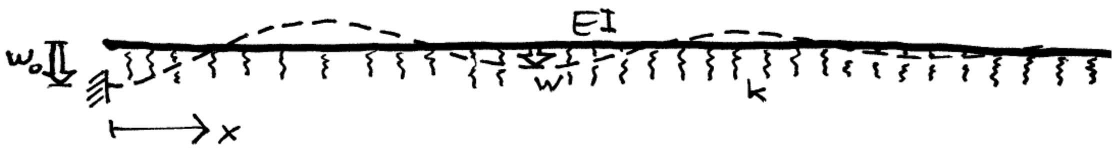

Figure 95. Beam supported by distributed springs and loaded by an imposed displacement w_0

The solution is

$$w = w_0 \left(\sin\frac{\pi x}{l_i} + \cos\frac{\pi x}{l_i}\right) \exp\frac{-\pi x}{l_i},$$

where

$$l_i = \sqrt{2}\,\pi \sqrt[4]{\frac{EI}{k}}$$

is the halve wave length.

Figure 96 shows displacement w, moment $M = -EI\dfrac{\partial^2 w}{\partial x^2}$ and shear force $V = \dfrac{\partial M}{\partial x}$.

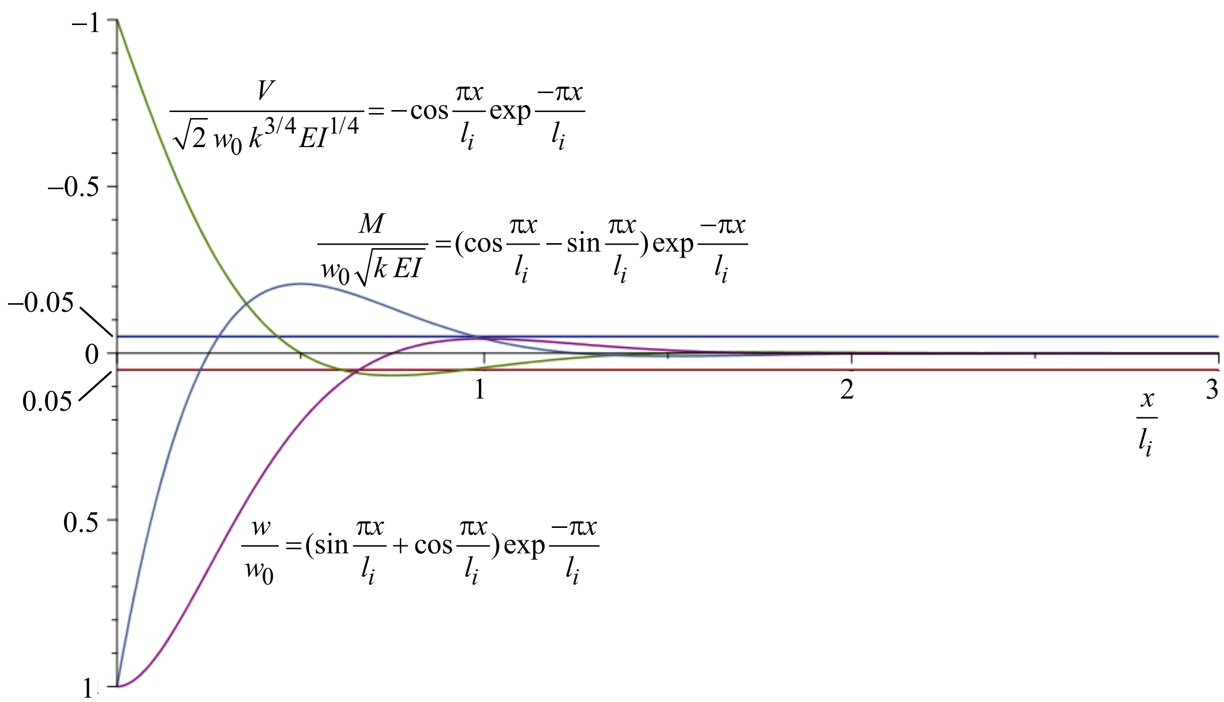

Figure 96. Displacement w, moment M and shear force V in the beam

Exercise: Suppose that the beam end is not fixed but pinned. What is the ratio of the pinned largest moment and the fixed largest moment?

Exercise: Suppose that the imposed displacement is removed, the left beam end is fixed and a uniformly distributed load q is applied to the beam. What changes to the differential equation, boundary conditions and solution?

Influence length
In figure 96 we see that the peak values occur at the left beam end. At some distance from the end the values are much smaller. At a distance $x = l_i$, all values are a bit smaller than 5% of the peak values (ignoring the signs). This distance is called the influence length. The influence length happens to be the same as the halve wave length l_i.

Exercise: What is the exact value of "a bit smaller than 5%" ?

Influence length of a cylinder edge
Consider a circular cylinder (fig. 97).

$$k_{xx} = 0 \qquad k_{yy} = \frac{-1}{a} \qquad k_{xy} = 0 \qquad \alpha_x = 1 \qquad \alpha_y = 1$$

An axial symmetric displacement is described by

$$u_x = -\frac{\nu}{a}\int w(u)du \qquad u_y = 0 \qquad u_z = w(u) \qquad p_z = 0$$

Please note the difference between ν (Poisson's ratio) and v (curvilinear coordinate). Surface load is not applied $p_z = 0$. These 9 equations have been substituted in the Sanders-Koiter equations (p. 54). The result is (see derivation in appendix 5)

$$\frac{Et^3}{12(1-\nu^2)}\frac{d^4w}{du^4} + \frac{Et}{a^2}w = 0$$

This is the same differential equation as that of a beam supported by springs (p. 71). Apparently we can make the following interpretation.

$$\frac{Et^3}{12(1-\nu^2)} = EI \qquad \frac{Et}{a^2} = k$$

Using the analogy, the influence length of a cylinder edge is

$$l_i = \sqrt{2}\,\pi\sqrt[4]{\frac{EI}{k}} = \frac{\pi}{\sqrt[4]{3(1-\nu^2)}}\sqrt{a\,t} \qquad \boxed{l_i \approx 2.4\sqrt{a\,t}}$$

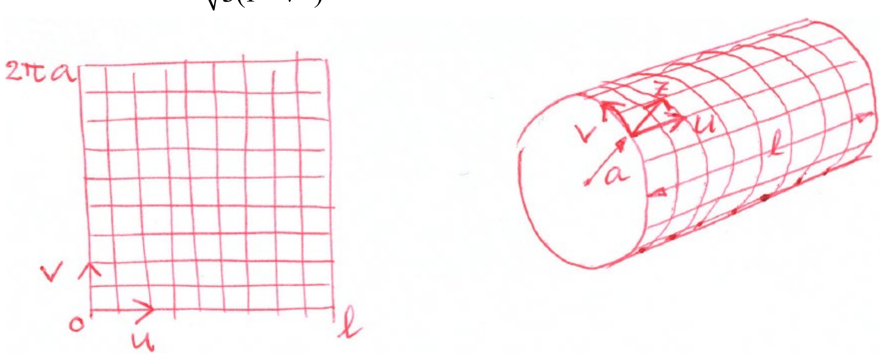

Figure 97. Cylinder parameterisation and dimensions

Exercise: Apparently, a shell can be sometimes interpreted as a beam supported by uniformly distributed springs. Which shell part is the beam and which shell part are the springs?

Influence lengths of all shells
Figure 98 gives influence lengths of edges of elementary shells. In more complicated shells the influence length of edge disturbances (p. 14, 71) can be estimated by comparing to the elementary shell shapes.

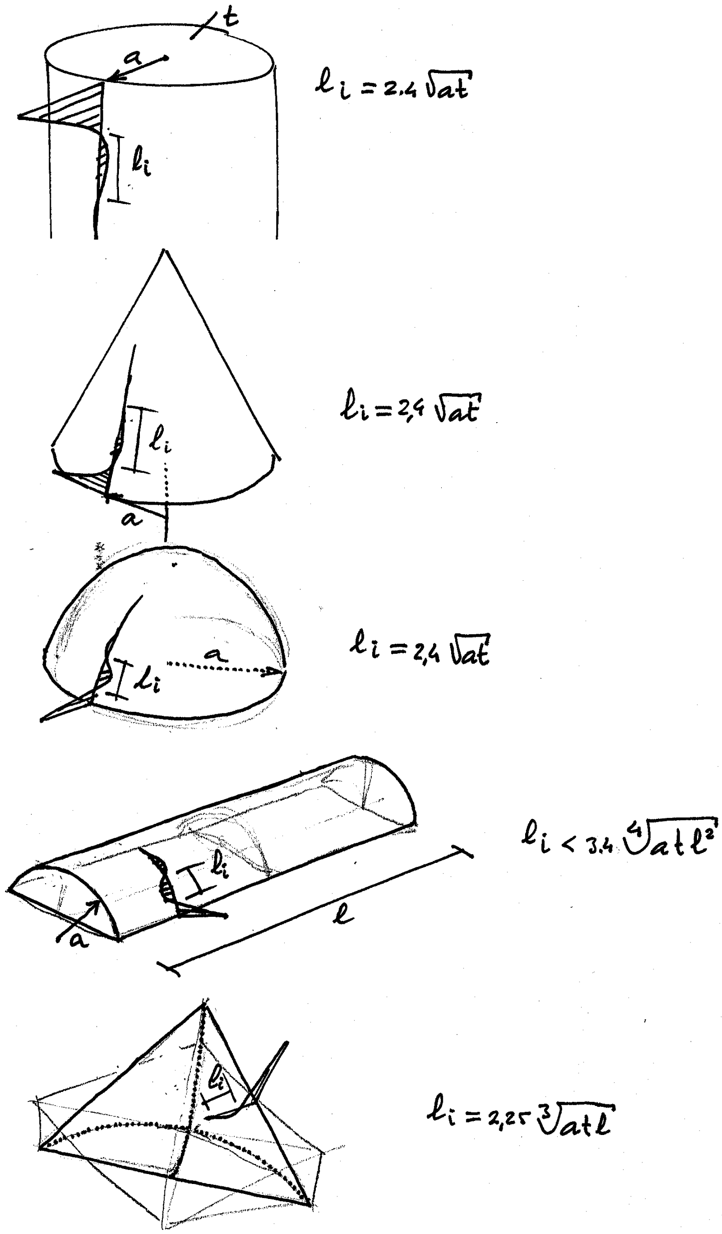

Figure 98. Influence lengths of elementary shell shapes [40]

Finite element mesh
The influence length can be used to choose a finite element mesh (p. 11, 84). If we use elements that approximate a solution linearly we need at least 6 elements in a length l_i in order to obtain

solutions with some accuracy (fig. 99). This provides a rule for the finite element length perpendicular to a shell discontinuity. Clearly, smaller elements will improve the accuracy.

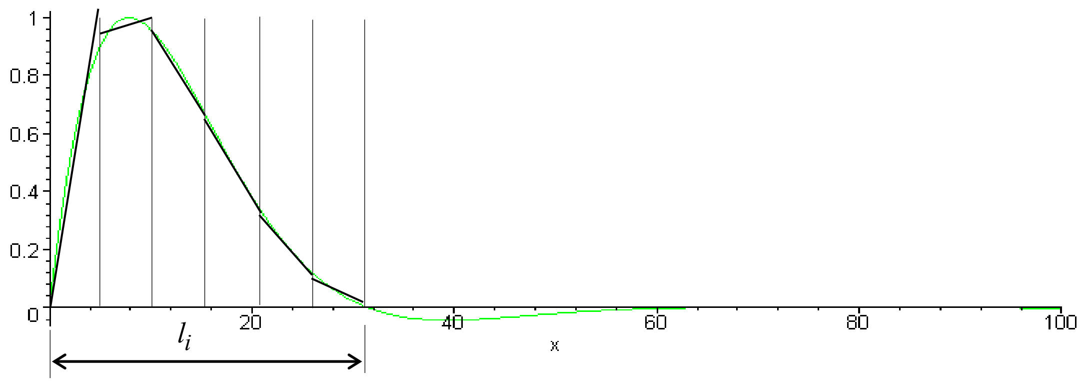

Figure 99. Piece-wise linear approximation of a solution

Exercise: For plates the recommended element size is 2*t*. Suppose that a shell needs elements this size. What is the *a/t* ratio of this shell? Is this a thin or a thick shell? Do thinner shells need smaller or larger elements than 2*t* ?

Boiler drums

Cylindrical boiler drums are made to contain pressurised water. The connection between the cylinder and a cap is an edge disturbance (p. 71). This edge disturbance can be analysed manually due to the axial symmetry in geometry and loading [40]. Figure 100 and 101 show results for different cap shapes. Figure 100 shows C_1 continuity (p. 11). Figure 101 shows C_0 continuity. The displayed membrane stresses are in the hoop direction. The displayed moments are in the meridional direction. In figure 100 the stress due to the maximum moment is approximately 30% of the stress due to the membrane force in the same direction. In figure 101 the stress due to the maximum moment is approximately 11 times the stress due to the membrane force in the same direction. Consequently, the drum in figure 101 is likely to yield when pressurised. This does not result in failure because the membrane forces continue to carry the load. For repeated loading fatigue will be a problem. Therefore, drum caps as in figure 101 are rarely applied.

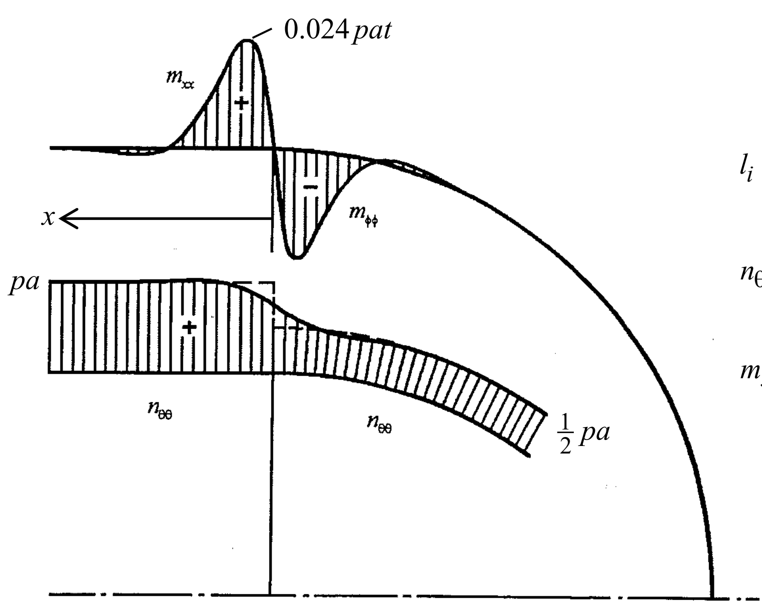

$$l_i = \frac{\pi}{\sqrt[4]{3(1-\nu^2)}}\sqrt{at}$$

$$n_{\theta\theta} = pa\left(1 - \tfrac{1}{4}\sin\frac{\pi x}{l_i}\exp\frac{-\pi x}{l_i}\right)$$

$$m_{xx} = \frac{pl_i^2}{8\pi^2}\sin\frac{\pi x}{l_i}\exp\frac{-\pi x}{l_i}$$

Figure 100. Membrane forces and moments in a hemispherical drum cap (v = 1/3 and a / t = 100) [40 p. 175]

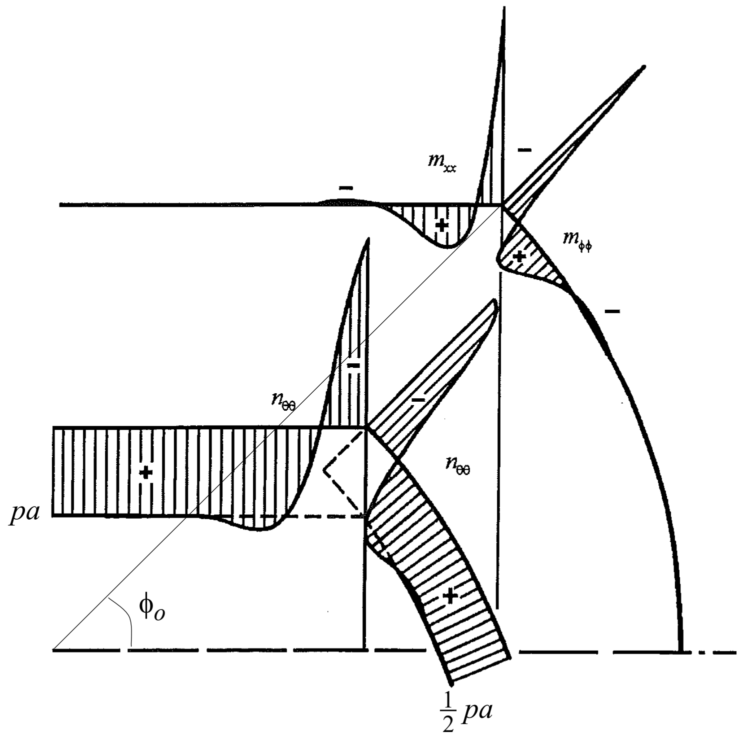

$$l_i = \frac{\pi}{\sqrt[4]{3(1-\nu^2)}} \sqrt{\frac{a\,t}{\sin\phi_o}}$$

$$m_{xx(x=0)} = \frac{-\cos\phi_o}{1+\sqrt{\sin\phi_o}} \frac{p\,a\,l_i}{4\pi}$$

Figure 101. Membrane forces and moments in a shallow drum cap (v = 1/3, a / t = 100 and ϕ_o = p / 4*) [40 p. 182]*

Saturn V
The rocket that brought people to the moon and back was called Saturn V (pronounce Saturn five). More than 20 Saturn Vs were built between 1965 and 1975. The parts were made by American aircraft companies. The Douglas Aircraft Company made an important part called S-IVB (pronounce S4B). It consisted of 8 shells and an engine (figs 99, 100). Note that the wall of the fuel tank is also the wall of the rocket. NASA made a rough design of S-IVB and specified the loads. The loads included an acceleration of 5 m/s^2, a fuel pressure of 6 bar and a fuel temperature of -253 ^{o}C. The engineers of Douglas designed the details and did a lot of testing [41, 42]. In the process they came up with orthogrid and isogrid (p. …).

Exercise: The Saturn V rockets were not reusable. The cost of each launch was 185 10^6 dollar [Wikipedia]. Suppose that all costs in the end are labour cost. Suppose that all people make approximately the same hourly salary. What percentage of the USA population was working to launch Saturn Vs?

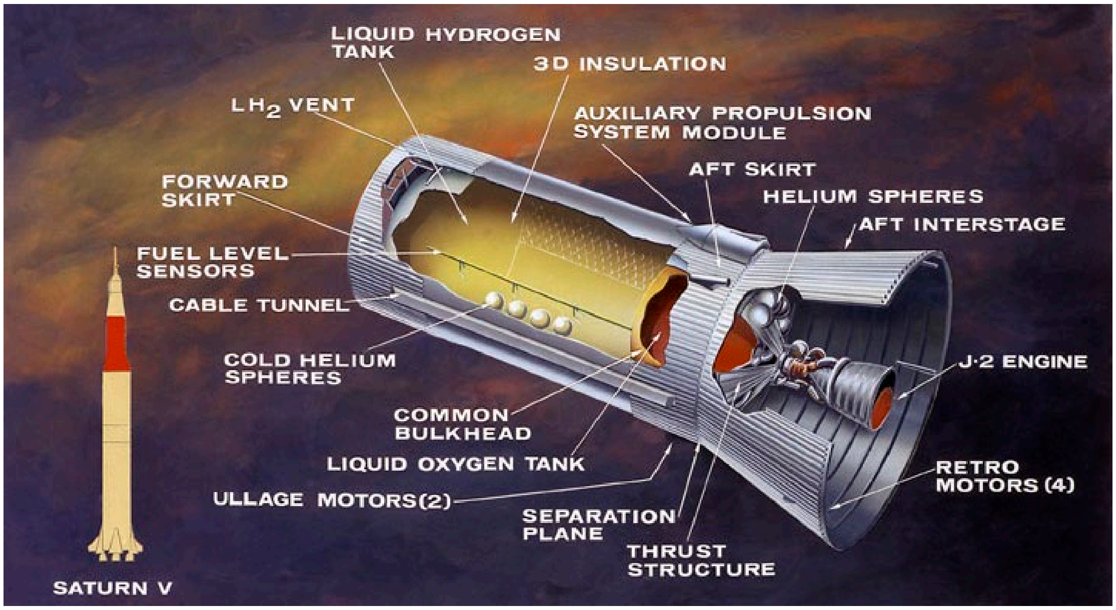

Figure 102. The S-IVB part of the Saturn V [Wikipedia]

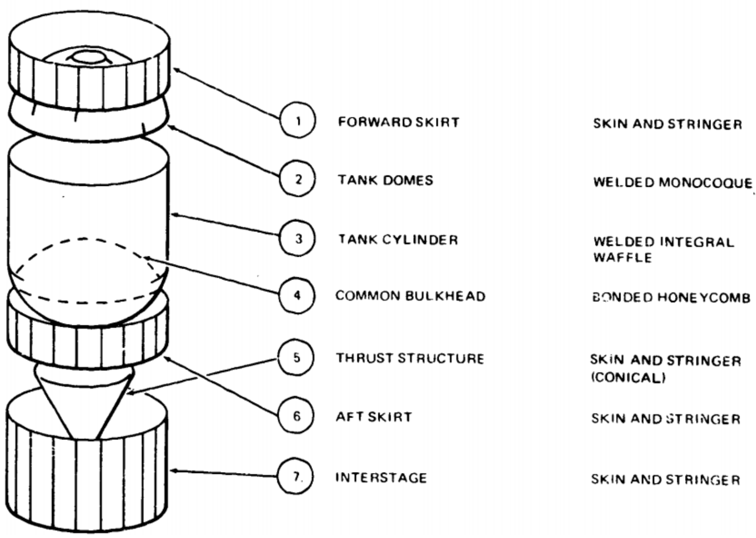

Figure 103. Shell components of S-IVB [41]

Literature

8 …, Differential geometry, …
9 C.R. Calladine, *Theory of Shell Structures*, Cambridge University Press,1983
10 … Queens palace …
11 … Florence …
12 … Florence …
13 St. Paul's cathedral, Gift shop booklet, Scala Publishers Ltd, London, 2011
14 St. Paul's cathedral, Gift shop poster, London, 1999
15 P.C.J. Hoogenboom, R. Spaan, "Shear Stiffness and Maximum Shear Stress of Round Tubular Members", 15th International Offshore and Polar Engineering Conference (ISOPE-2005), Seoul, June 19-24, 2005, Vol. 4, pp. 316-319
18 A.E.H. Love, "The Small Free Vibrations and Deformation of a Thin Elastic Shell", Philosophical Transactions of the Royal Society of London, Vol. 179, 1888, pp. 491-546
19 A.E.H. Love, "A treatise on the mathematical theory of elasticity", Cambridge University press, Volume 2, 1893
20 W. Flügge, "Statik und Dynamik der Schalen", Springer-Verlag, Berlin, 1934 (in German).
21 R. Byrne, "Theory of small deformations of a thin elastic shell", University of California, Publications in Mathematics (new series), 1944, Vol. 2, pp. 103-152.
22 E. Reissner, "Stress strain relations in the theory of thin elastic shells", *Journal of Mathematical Physics,* 1952, Vol. 31, pp. 109-119.
23 P.M. Naghdi, "On the theory of thin elastic shells", *Quarterly Applied Mathematics*, 1957, Vol. 14, pp. 369-380.
24 A.E.H. Love, "A treatise on the mathematical theory of elasticity", second edition, Cambridge University press, New York, 1906
25 J.L. Sanders, "An improved first approximation theory for thin shells", National Aeronautics and Space Administration (NASA) Report No. 24, Washington, DC, 1959.
26 W.T. Koiter, "A consistent first approximation in the general theory of thin elastic shells", Report, Delft University of Technology, 1959.
27 W.T. Koiter, "A consistent first approximation in the general theory of thin elastic shells", Proceedings of IUTAM Symposium "On the Theory of Thin Elastic Shells", Delft 24-28 August 1959, North-Holland publishing company, Amsterdam 1960, pp 12-33.
28 D.H. van Campen, "Levensbericht W.T. Koiter", Huygens Institute - Royal Netherlands Academy of Arts and Sciences (KNAW), *Levensberichten en herdenkingen*, 1999, Amsterdam, pp. 7-12
29 L.H. Donnell, "A new theory for the buckling of thin cylinders under axial compression and bending", *Transactions of the American Society of Mechanical Engineers*, 1934, Vol. 56, pp. 759-806.
30 L.S.D. Morley, "An improvement on Donnell's approximation for thin-walled circular cylinders", *Quarterly Journal of Mech. Applied Mathematics*, 1959, Vol. 12 (Part 1), pp. 89-99.
31 Anonymous, *Caltech Alumni News*, December 1948, online (20-08-2022) https://calteches.library.caltech.edu/642/2/Alumni.pdf, excerpt: "J.H. Wayland, M.S. '35, PhD. '36, has been appointed Associate Professor of Applied Mechanics at the Institute, to succeed Ralph E. Byrne, Jr., who died on September 17."
32 Anonymous, *1940 U.S. Census*, online (20-08-2022) https://www.ancestry.com/1940-census/usa/California/Ralph-E-Byrne-Junior_2j5w9x, excerpt: "… Age 28, born abt 1912, Birthplace Missouri, Gender Male, Race White, Home in 1940 803 South Oakland Avenue Pasadena …,"
34 J. Blaauwendraad, *Plates and FEM, Surprises and Pitfalls*, Springer, 2010, p 77.
35 R. Zwennis, Spanningen in de rand van koud vervormde glasplaten, Bachelor's project, Delft University of Technology, June 2013, (In Dutch), online: http://homepage.tudelft.nl/p3r3s/BSc_projects/eindrapport_zwennis.pdf

36 … palazetto dello sport, …
37 …
38 …
39 …
40 J. Blaauwendraad, J.H. Hoefakker, *Structural Shell Analysis, Understanding and Application*, Springer, 2014, 305 pp.
41 H.W. Babel, R.H. Christensen, H.H. Dixon, Design, fracture control, fabrication, and testing of pressurized space-vehicle structures, Chapt 23 in Thin-shell structures; Theory, experiment and design, Y.C. Fung, E.E. Sechler (editors) Prentice-Hall, New Jersey, 1974.
42 Anonymous, Isogrid design handbook, McDonnel Douglas Astronautics Company, California, 1973

Appendix 4. Compatibility equation

In this appendix the shell compatibility equation (p. 57) is checked.

```
> ux:=  c1 +   c2*u +   c3*v +   c4*u^2 +   c5*u*v +   c6*v^2 +   c7*u^3 +   c8*u^2*v +   c9*u*v^2 + c10*v^3:
> uy:=c11 + c12*u + c13*v + c14*u^2 + c15*u*v + c16*v^2 + c17*u^3 + c18*u^2*v + c19*u*v^2 + c20*v^3:
> uz:=c21 + c22*u + c23*v + c24*u^2 + c25*u*v + c26*v^2 + c27*u^3 + c28*u^2*v + c29*u*v^2 + c30*v^3:
> epsilonxx:=diff(ux,u)/alphax-kxx*uz+kx*uy:
> epsilonyy:=diff(uy,v)/alphay-kyy*uz+ky*ux:
> gammaxy:=diff(ux,v)/alphay+diff(uy,u)/alphax-2*kxy*uz-kx*ux-ky*uy:
> phix:=-diff(uz,u)/alphax-kxx*ux-kxy*uy:
> phiy:=-diff(uz,v)/alphay-kyy*uy-kxy*ux:
> phiz:=1/2*(-diff(ux,v)/alphay+diff(uy,u)/alphax-kx*ux+ky*uy):
> kappaxx:=diff(phix,u)/alphax-kxy*phiz+kx*phiy:
> kappayy:=diff(phiy,v)/alphay+kxy*phiz+ky*phix:
> rhoxy:=diff(phix,v)/alphay+diff(phiy,u)/alphax+(kxx-kyy)*phiz-kx*phix-ky*phiy:
> l:=-diff(epsilonxx,v,v)/alphay^2 + diff(gammaxy,u,v)/alphax/alphay - diff(epsilonyy,u,u)/alphax^2:
> r:=-kyy*kappaxx + kxy*rhoxy - kxx*kappayy:
> u:=0: v:=0: kx:=0: ky:=0: kxx:=kxy^2/kyy:
> simplify(l-r);
                    0
```

Q.E.D.

Appendix 5. Cylinder equation

In this appendix the shell cylinder equation (p. 73) is derived.

```
> ux:=-nu/a*int(w(u),u): uy:=0: uz:=w(u):
> pz:=0:
> kxx:=0: kyy:=-1/a: kxy:=0: alphax:=1: alphay:=1:
> ky:=diff(alphay,u)/alphay/alphax: kx:=diff(alphax,v)/alphax/alphay:
> epsilonxx:=diff(ux,u)/alphax-kxx*uz+kx*uy:
> epsilonyy:=diff(uy,v)/alphay-kyy*uz+ky*ux:
> gammaxy:=diff(ux,v)/alphay+diff(uy,xs)/alphax-2*kxy*uz-kx*ux-ky*uy:
> phix:=-diff(uz,u)/alphax-kxx*ux-kxy*uy:
> phiy:=-diff(uz,v)/alphay-kyy*uy-kxy*ux:
> phiz:=1/2*(-diff(ux,v)/alphay+diff(uy,u)/alphax-kx*ux+ky*uy):
> kappaxx:=diff(phix,u)/alphax-kxy*phiz+kx*phiy:
> kappayy:=diff(phiy,v)/alphay+kxy*phiz+ky*phix:
> rhoxy:=diff(phix,v)/alphay+diff(phiy,u)/alphax+(kxx-kyy)*phiz-kx*phix-ky*phiy:
> nxx:=E*h/(1-nu^2)*(epsilonxx+nu*epsilonyy):
> nyy:=E*h/(1-nu^2)*(epsilonyy+nu*epsilonxx):
> nxym:=E*h/(2*(1+nu))*gammaxy:
> mxx:=E*h^3/(12*(1-nu^2))*(kappaxx+nu*kappayy):
> myy:=E*h^3/(12*(1-nu^2))*(kappayy+nu*kappaxx):
> mxy:=E*h^3/(24*(1+nu))*rhoxy:
> vx:=diff(mxx,u)/alphax+diff(mxy,v)/alphay+ky*(mxx-myy)+2*kx*mxy:
> vy:=diff(myy,v)/alphay+diff(mxy,u)/alphax+kx*(myy-mxx)+2*ky*mxy:
> nz:=(kxy*(mxx-myy)-(kxx-kyy)*mxy)/2:
> nxy:=nxym-nz:
> nyx:=nxym+nz:
> px:=-(diff(nxx,u)/alphax+diff(nyx,v)/alphay+ky*(nxx-nyy)+kx*(nxy+nyx)-kxx*vx-kxy*vy):
> py:=-(diff(nyy,v)/alphay+diff(nxy,u)/alphax+kx*(nyy-nxx)+ky*(nxy+nyx)-kyy*vy-kxy*vx):
> pz:=-(kxx*nxx+kxy*(nxy+nyx)+kyy*nyy+diff(vx,u)/alphax+diff(vy,v)/alphay+ky*vx+kx*vy):
> simplify(px);
```

$$0$$

```
> simplify(py);
```

$$0$$

```
> collect(simplify(pz),w(u));
```

$$\frac{Eh}{a^2}w(u)+\frac{Eh^3}{12(1-\nu^2)}\left(\frac{d^4}{du^4}w(u)\right)$$